Spring 4-16-2021

Characterizing Solute Transport and Processing Dynamics in the Headwaters of the South River (South Atlanta, GA, USA)

Christopher Wheeler

CHARACTERIZING SOLUTE TRANSPORT AND PROCESSING DYNAMICS IN THE HEADWATERS OF THE SOUTH RIVER (SOUTH ATLANTA, GA, USA)

by

CHRISTOPHER THOMAS WHEELER

Under the Direction of Sarah H. Ledford, PhD

ABSTRACT

Urban development has degraded numerous headwater streams. Objectives of this study are: (1) to characterize variation in baseflow hydrochemistry in headwater streams of the South River Watershed (Atlanta, GA, USA) and relate it to differences in land use and other characteristics, as well as to (2) examine solute dynamics during storm events. Results suggest that land use on the watershed scale has a significant influence on mean baseflow nitrate concentration at a given site, with antecedent precipitation also playing a role. Additionally, we collected samples throughout storm events at three USGS stream gage sites. Water chemistry data was paired with USGS discharge and specific conductivity measurements to create concentration-discharge plots. Results from both baseflow and stormflow sampling suggest that, within this watershed, maximum solute concentrations at any location are generally observed at baseflow. As such, this is a source-limited system where groundwater also represents the highest-concentration component of storm flow.

INDEX WORDS: Urban Hydrology, Watershed biogeochemistry, C-Q relationships, Land use, Solute Dynamics, Headwater study, C-Q hysteresis, Storm event-scale

CHARACTERIZING SOLUTE TRANSPORT AND PROCESSING DYNAMICS IN THE HEADWATERS OF THE SOUTH RIVER (SOUTH ATLANTA, GA, USA)

by

CHRISTOPHER THOMAS WHEELER

A Thesis Submitted in Partial Fulfillment of the Requirements for the Degree of

Master of Science

in the College of Arts and Sciences

Georgia State University

2021

CHARACTERIZING SOLUTE TRANSPORT AND PROCESSING DYNAMICS IN THE HEADWATERS OF THE SOUTH RIVER (SOUTH ATLANTA, GA, USA)

by

CHRISTOPHER THOMAS WHEELER

Committee Chair: Dr. Sarah H. Ledford

Committee: Dr. Sarah H. Ledford

Dr. Richard Milligan

Dr. Luke Pangle

Electronic Version Approved:

Office of Graduate Services

College of Arts and Sciences

Georgia State University

May 2021

DEDICATION

I would like to dedicate this to my parents, Mark and Laurie Wheeler, as well as my partner Diana Alatorre, for their encouragement, support, and belief in me.

ACKNOWLEDGEMENTS

I would first like to thank my advisor, Dr. Sarah H. Ledford, for her immense level of assistance, encouragement, support, and patience, and the very large amount of time spent assisting me with both my research and professional development. I would also like to thank Dr. Luke Pangle and Dr. Richard Milligan, for their help on this project and my academic and professional development. Additionally, I would like to thank all of my colleagues in the Geosciences Department and Water Science concentration for their support and friendship.

TABLE OF CONTENTS

LIST OF TABLES

LIST OF FIGURES

LIST OF ABBREVIATIONS

µS/cm: Microsiemens per centimeter (unit of specific conductivity)

2CM: 2-Component mixing model

3CM: 3-Component mixing model

Baltimore LTER: Baltimore Long-term Ecologic Research Site

BES: Baltimore Ecosystem Study

C-Q: Concentration-Discharge

CSO: Combined sewer overflow

DO: Dissolved oxygen (measured in % saturation for this study)

ISC: Impervious surface coverage

LULC: Land use and land cover

mg/L: Milligram per liter (unit for sample concentrations)

MRLC: Multi-Resolution Land Characteristics Consortium

N: denoting the element nitrogen

NLCD: National Land Cover Database

NO_3^-: denoting the ionic compound nitrate

P: denoting the element phosphorus

Q: denoting stream discharge (L^3/T)

SPC: Specific Conductivity of Specific Conductance

USGS: United States Geological Survey

1 INTRODUCTION

1.1 Urban stream degradation

Urbanization has proven to represent the dominant demographic paradigm of the 21st century. As of 2008, over half of the world's population lives in urban areas, and specific mechanisms and processes associated with urbanization (both demographically/sociologically and regarding natural systems) have proven heterogeneous and warrant further study (Bloom et al., 2008). In particular, urbanization has significantly, and at times systematically, altered natural systems, including low order urban streams. Observed adverse effects on such urban headwaters include systemic hydraulic, ecologic, and hydrochemical degradation (Meyer et al., 2005). In terms of changes in chemistry, urbanization has been shown to significantly increase concentrations of nutrients (e.g., nitrogen (N) and phosphorous (P) concentrations) (Walsh et al., 2005). This headwater degradation can ultimately affect the larger, downstream water bodies to which the low-order streams contribute.

Ecologists and hydrologists have recognized and begun to evaluate a consistent set of "symptoms" associated with streams draining urban catchments, which was ultimately termed the "urban stream syndrome" by Walsh et al. (2005). These systematic symptoms of degradation include flashier hydrographs compared to forested counterparts, higher nutrient and contaminant concentrations, and incision/destabilization of stream channels, among other phenomena (Meyer et al., 2005; Paul and Meyer, 2001). Impervious surface cover (ISC) is one of the key factors driving those changes. ISC represents the percentage of a catchment covered with concrete, buildings, or other material that prevent or impede infiltration of precipitation, and it is often discussed as a critical driver of altered hydrologic response and hydrochemistry in urban systems (Arnold and Gibbons, 1996; Brabec et al., 2002). In the southeastern United States, which is

located in a humid subtropical climate zone, urbanization has been shown to have a dramatic effect on peak flows, significantly increasing runoff ratios (O'Driscoll et al., 2010). Numerous negative externalities are associated with degradation of urban streams, including widespread eutrophication of larger downstream water bodies as one of the most serious consequences (Baker et al., 2001; Shields et al., 2008; Smith et al., 2003).

1.2 Urban streams in the Atlanta area

Following the worldwide trend of urbanization, the Atlanta Metropolitan Region (AMR), which consists of 10 counties, experienced nearly a 100% growth in population from 1970 to 1995 (Gregory and Frick, 2000). This growth has caused significant ecological stress to the natural environment via rapid increases in residential and industrial development, as well as in the magnitude of ISC (Gregory and Frick, 2000). This high level of urban development is compounded by Atlanta's early history of installing combined sewer systems that resulted in combined sewer overflows (CSOs) for stormwater control/management instead of entirely separate systems for wastewater and stormwater control (Frick et al., 1998).

In Atlanta, multiple studies confirm the presence of typical stream impacts associated with urbanization, including changes in baseflow, stream solutes, and storm flow. Across the Upper Chattahoochee River Basin, watersheds representing a wide range of urban development showed significant increases in baseflow concentrations of solutes with increasing levels of urbanization (Rose, 2007). Additionally, baseflow concentrations were significantly higher for any level of urbanization when compared to the rural sites. Rose (2007) hypothesized that diffusive (non-point) sources of waste (via leaky sewer infrastructure) were the major drivers of elevated solute levels at the urban sites, along with proximity to combined sewer overflows. In addition to elevated solute concentrations, urbanization in the Atlanta area has led to dramatic

alteration of natural flow regimes. Rose and Peters (2001) showed the highly urbanized Peachtree Creek exhibited peak flows 30% to 100% larger than the forested sites used for comparison in the study—a result that is consistent with most comparative urban-forest watershed studies. Stream discharge at Peachtree Creek also decreased much more rapidly after storm events, as quantified by storm recession constants that were significantly greater than the forested sites in this study. This indicates that urbanization has caused an increase in hydrograph "flashiness" for Peachtree Creek, as expected. This was confirmed to continue to be the case almost 20 years later, when Diem et al (2017) showed that increased urbanization in the Metropolitan area exhibited increased flashiness. Furthermore, Rose and Peters (2001) showed low flows at Peachtree Creek were 25% to 30% lower than at the other sites, which was also confirmed by Diem et al (2017). Although reduction in low flows is sometimes cited as a general characteristic of urban stream degradation (Walsh et al., 2005) others have questioned the universality of this urban stream "symptom" by showing that leaky stormwater infrastructure in cities can ultimately increase baseflow (Ledford et al., 2020; Bhaskar et al., 2020). Finally, although urbanization is expected to increase runoff coefficients (the percentage of precipitation that becomes stormwater runoff) in streams (Paul and Meyer, 2001), Diem et al. (2017) found that watershed slope was the primary control on this parameter, rather than urbanization.

1.3 Previous work on urban N dynamics

Several studies have attempted to understand the impacts of urbanization on overall stream health through measurements of nutrient loading, processing, and export at multiple scales. Nutrient loading refers to the mass of a single solute or set of solutes (i.e., nutrients) that enters a particular ecosystem or watershed during a pre-defined period. Similarly, nutrient export is defined as the mass of a single solute or set of solutes that exits a particular ecosystem or

watershed during a pre-defined period (Smith et al., 2003). Furthermore, nutrient retention refers to the fraction of mass of a nutrient or set of nutrients that remains in a watershed or ecosystem, calculated by accounting for combined loading and export (i.e., retention = 1 – export/loading) (Wollheim et al., 2005). Although highly scale and site-dependent, the most general trend found in comparative urban watershed studies is significantly higher nutrient loading than in forested counter parts. This higher loading is generally attributed to elevated anthropogenic sources (Mulholland et al., 2008; Vitousek et al., 1996) and changes in riparian characteristics and canopy cover (Grimm et al., 2005; O'Driscoll et al., 2010), while decreased retention is impacted by decreased channel complexity and changes in light exposure, ecosystem productivity, and respiration (Ledford et al., 2017).

In terms of nitrogen (N) and nitrate (NO_3^-) dynamics, a study by Wollhiem et al. (2005) found that N retention in urban streams remained unexpectedly high when compared to forested counterparts, possibly because N loading peaks at approximately 30% ISC, then declines, while runoff continues to increase. Examining diffuse N export related to discharge, Shields et al. (2008) performed a study utilizing catchments from the Baltimore Ecosystem Study, attempting to parse how N export changes with flow magnitude and at different levels of urbanization. The study found that more urbanized sites exhibit a majority of N export occurring during high flows, while the less developed sites exhibit most N export at relatively low flows. In a similar investigation of diffuse N dynamics at the Baltimore long-term Ecological Research Site, Kaushal et al. (2011) incorporated stable isotopes along with an N budget approach to further characterize N sources and speciation. Through examination of N isotope values, the authors found that while wastewater was the dominant source at baseflow, atmospheric and agricultural

sources began to contribute more as discharge increased during storm events. Isotope analysis also revealed widespread denitrification occurring for wastewater and agricultural N.

1.4 Concentration-discharge (C-Q) relationships & C-Q hysteresis

Recently, many studies have examined the hysteretic relationship between discharge and various solute concentrations in lotic systems. These are often termed concentration-discharge (C-Q) relationships (Koenig et al., 2017). Examining these relationships for storm events can help reveal catchment-wide solute mobilization and transport processes (Lloyd et al., 2016). In addition to mixing model concentration rankings (Evans and Davies, 1998), the analysis of hysteresis loops can also provide more general information about how a specific solute behaves in a catchment. The slope of the C-Q loop indicates whether a solute is "source limited" (exhibits dilution behavior) or "transport limited" (exhibits flushing behavior) during a storm event. Positive slopes represent flushing, while negative slopes represent dilution (Aguilera and Melack, 2018; Bowes et al., 2005). Additionally, loops showing clockwise rotation indicate that concentration peaks while the storm hydrograph is rising. Clockwise rotation is usually interpreted as an indication that the solute source is spatially close to the stream. Conversely, an anticlockwise pattern indicates a solute source further from the stream, resulting in peak concentrations while the storm hydrograph is falling (Evans and Davies, 1998).

Since Evans and Davies (1998), numerous C-Q hysteresis studies have been performed on the storm event scale. Additionally, various hysteresis indices (most incorporating some form of normalized concentration and discharge values) have been developed to more effectively compare responses between storms and catchments (Lloyd et al., 2016; Zuecco et al., 2016). Using such a methodology, Aguilera and Melack (2018) classified approximately 400 storm events over 13 years at 10 sampling sites. The authors used a combined approach that indexed and compared the

slope and rotational pattern for each loop. Variation in the results was shown to be controlled mainly by land use and land cover (LULC), as well as antecedent moisture conditions (often varying seasonally). Other studies have used similar methods to parse spatial and temporal dynamics controlling mechanisms for multiple solutes at various levels of urbanization (Bowes et al., 2005; Bieroza and Heathwaite, 2015; Baker and Showers, 2019). Although analysis of C-Q hysteresis loops has proven to be a powerful analytic tool for investigation of catchment-scale solute dynamics, multiple assumptions are inherent in this method, and they should be considered prior to utilization. Evans and Davies (1998) used a representative hydrograph that assumed a specific relative magnitude and timing for each component of stormflow, utilizing a 3-Componoent Model (3CM). Subsequent studies have shown that even small variations in these assumptions can confound estimates of component concentration rankings in such mixing models (Scanlon et al., 2001; Chanat et al., 2002; Hornberger et al., 2001). Additionally, others have speculated that in some watersheds, storm-event-solute responses can be modeled more accurately by using a two-component mixing model (2CM), rather than a 3CM. In a 2CM, soil water composition is viewed as almost identical to that of groundwater, rather than being quantified as a distinct reservoir (Rose, 2003).

Although numerous C-Q hysteresis studies have been performed in forested, agricultural, and urban settings across a wide range in physiographic and climatic settings, hysteresis data from urban watersheds in Atlanta is lacking. However, multiple C-Q studies have been performed at the Panola Mountain Research Watershed, a forested hydrologic research site in the Atlanta area (Aulenbach, 2014; Carroll, 2007). Rose (2003) represents the most thorough existing hysteresis study of a developed, low-order watershed in Atlanta. Using the Evans and Davies (1998) typology as a conceptual model, this study examined solute dynamics in the highly developed Peachtree

Creek watershed and compared results with a less developed reference catchment. Despite sampling for a wide variety of chemistries, storm event C-Q patterns were remarkably consistent in Peachtree Creek. Hysteresis loops in Peachtree Creek exhibited an almost exclusively clockwise rotational pattern (indicating proximal solute sources), as well as an almost exclusively negative slope (indicating a source-limited, dilution response to increasing discharge).

Although urban C-Q studies in Atlanta remain relatively sparse, there is a growing body of work aimed at studying the effects of hydraulic and chemical changes, driven by urbanization, on C-Q relationships in a diverse array of physiographic and climatic settings, and at various spatiotemporal scales (Duncan et al., 2017; Thompson et al., 2010; Gwenzi et al., 2017). Some studies have attempted to measure variation in C-Q responses across gradients of urbanization, finding key differences in slope and rotational direction between urban and forested sites on the storm event scale (Aguilera and Melack, 2019). Other studies have compared C-Q relationships at the same study site but at different temporal scales (Duncan et al., 2017). Such studies have often noted a "threshold-like" transition in discharge magnitude for which metrics such as slope and rotational direction change (Thompson et al., 2010; Gwenzi et al., 2017).

1.5 Objectives of study

Given the history of development in Atlanta and its rapid continuing growth, understanding both sources and transport mechanisms for contaminants on the watershed scale is crucial for future mitigation efforts. In particular, low order streams (headwaters) have been shown to have pronounced importance (as well as substantial spatial and temporal heterogeneity) in terms of nutrient loading and other dynamics for the larger order streams and rivers that are fed by these systems (Peterson et al., 2001). Examining solute dynamics on the storm event scale is another matter of importance for mitigation, as storm events often account for a large

proportion of nutrient fluxes in a watershed each year (Bell et al., 2008; Sebestyen et al., 2016). As such, this study has two motivating objectives: to characterize nutrient and major ion sources and retention in headwater streams of the South River watershed (South Atlanta, GA, USA), as well as to examine relationships between stream discharge and concentrations of various solutes during storm events.

2 METHODOLOGY

2.1 Characterization of geology, soils, and climate in the Georgia Piedmont

Most of northern Georgia, including the city of Atlanta (Rose and Peters, 2001), lies within the Piedmont physiographic province (Diem et al., 2017), as well as the humid subtropical Köppen climatic zone (O'Driscoll et al., 2010). As such, the climate of the Atlanta area is characterized by high humidity and temperatures in summer months, contrasted with cold and relatively mild winter months (Karl and Kloss, 1984). Per daily measurements at Fulton County Airport from 1981 to 2010, the Atlanta area experiences average air temperatures ranging from 0.61 °C (January) to 31.94 °C (July). Additionally, Atlanta receives an average total of 130 cm of precipitation per year (NOAA, 2020). Geologically, the province is characterized by a highly fractured and heterogeneous igneous and metamorphic bedrock layer of Paleozoic origin and felsic composition (e.g., granites, schists, gneisses) (Swain et al., 2004; Rose and Peters, 2001). This bedrock is overlain by a weathered regolith of largely the same composition, the lower portion of which is known as saprolite (Miller et al., 1990; Long and Baldwin, 1917). This saprolite is overlain by soils of essentially this same composition. However, surficial and near-surficial soils in this region can contain a substantial organic component, and respective depths to saprolite and bedrock are highly variable and dependent on topography (McIntosh et al., 1999; Miller et al., 1990). From a hydrogeologic perspective, this crystalline subsurface, although highly fractured and heterogeneous, has nonetheless proven unsuitable for large-scale groundwater extraction. Although the regolith is host to an extensive unconfined, surficial aquifer system, its volumetric yield is not sufficient for heavy industrial or agricultural uses (Miller et al., 1990).

2.2 Site description: South River Watershed (SRW)

The South River Watershed (Fig. 1) is located in the southeastern portion of the Metro-Atlanta area, principally in DeKalb County (Diem et al., 2017). In 2016, DeKalb County had a total population of 759,297 persons (US Census, 2016) and it encompasses an area of approximately 694 km^2 (Dai et al., 2019), with an average population density of 1,094 persons/km^2. Although originally forested, clearing (largely via controlled burns) and agricultural production, ultimately of cotton, began in the early 19th century. In terms of soils, DeKalb County is located entirely in the so-called "red hill" region of the northern Piedmont province (Long and Baldwin, 1917). With the exception of alluvium occurrences along stream bottoms, soils are largely residuals, which have been classified into numerous distinct types (Thomas, 1979). Most notably, the distinct "red clay" soils of the Cecil series formed via weathering of underlying granite, mica schist, gneiss, and hornblende schist (Long and Baldwin, 1917). However, continuous urbanization since the late 19th century has dramatically altered the landscape and hydrology of the entire Metro-Atlanta region, including the South River Watershed (Rose, 2002; Rose, 2007).

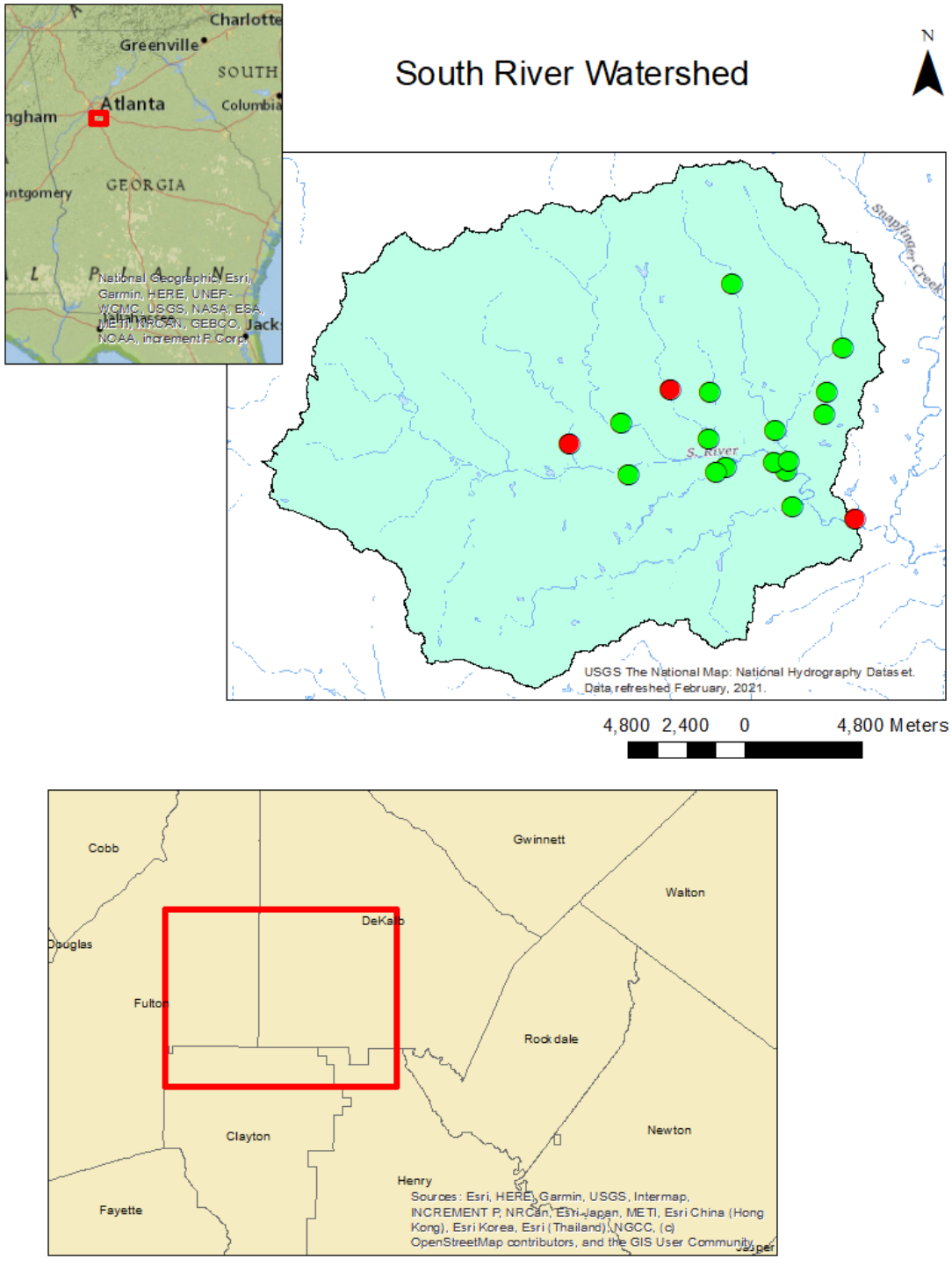

Figure 1: Extent of South River Watershed, with its location in Georgia in red (top-left). Bottom-left: map of metro-Atlanta counties with SRW location in red. Middle: map of the upper South River watershed, where green dots represent the location of baseflow sampling sites and red dots represent USGS gages used for storm event study, as well as baseflow sampling.

South River at Flakes Mill Road (Fig. 2) represents the pour point for the main watershed used in this study. The Intrenchment (Fig. 3) and Doolittle (Fig. 4) gages, along with all sampling sites in this study, are nested within the drainage basin associated with South River at Flakes Mill Road. Watershed drainage area for the USGS gages ranged from 11 to 256.4 km^2 (Table 1), with the smaller two watersheds (Intrenchment Creek and Doolittle Creek) having higher ISC than the overall larger South River (Table 2). The Intrenchment Creek gage is located directly downstream of the Custer Street and East Area CSO facilities. This site exhibits a substantially higher percentage of areal coverage by primary roads (2.35%) than the percentages for the other two gage sites (1.83% at South River and 1.36% at Doolittle Creek) (Table 3) Each of these three gages is maintained by DeKalb County, Georgia. The gages record precipitation, discharge, and specific conductivity (SPC) at 15-minute intervals.

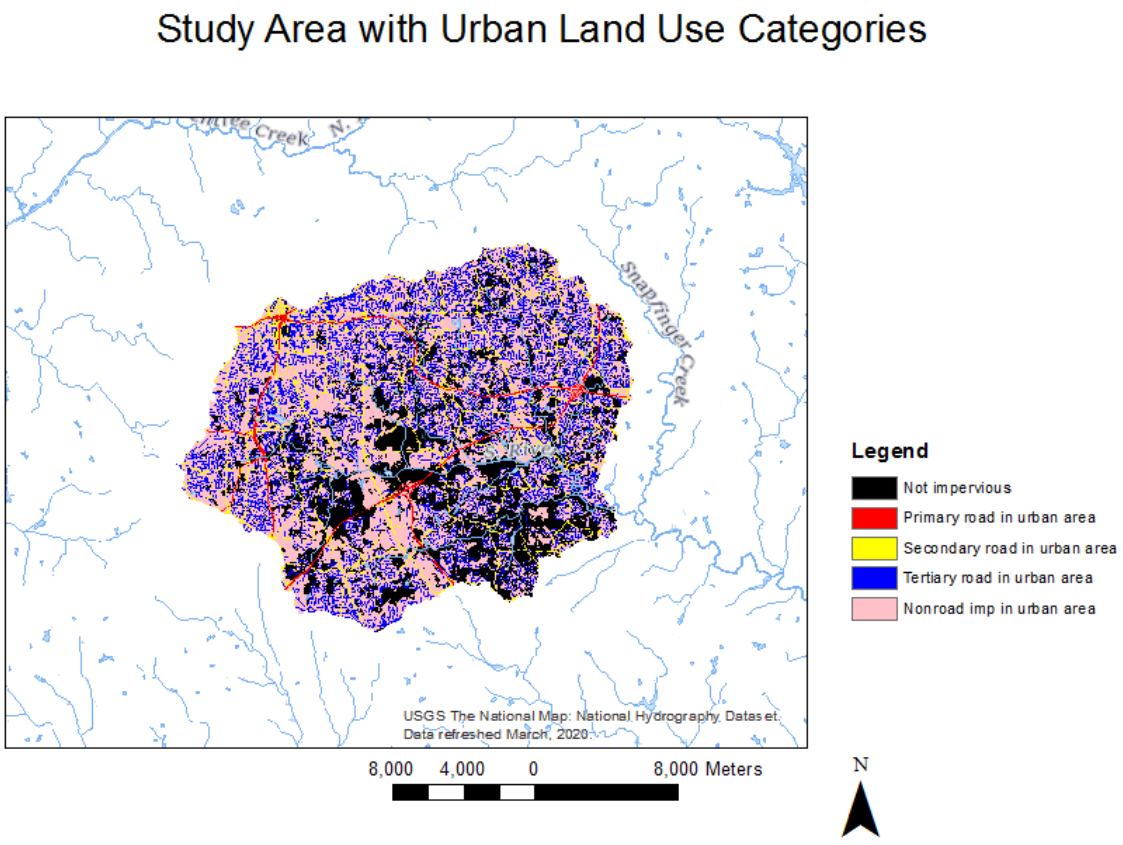

Figure 2:Outline of South River Watershed with Land Use Categories (NLCD 2016).

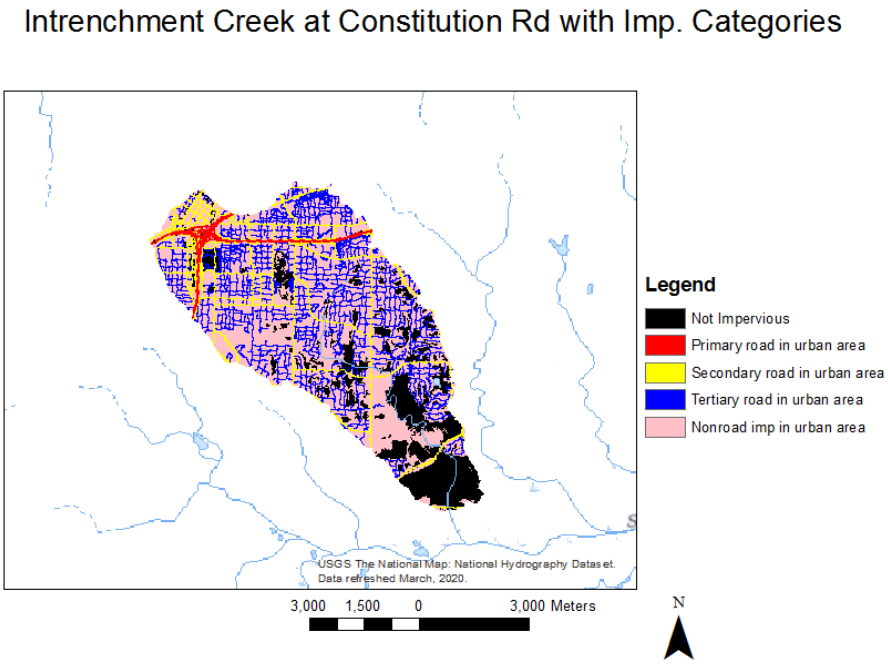

Figure 3: Outline of the drainage area for USGS 02203700 (Intrenchment Creek at Constitution Road) with Land Use Categories (NLCD 2016).

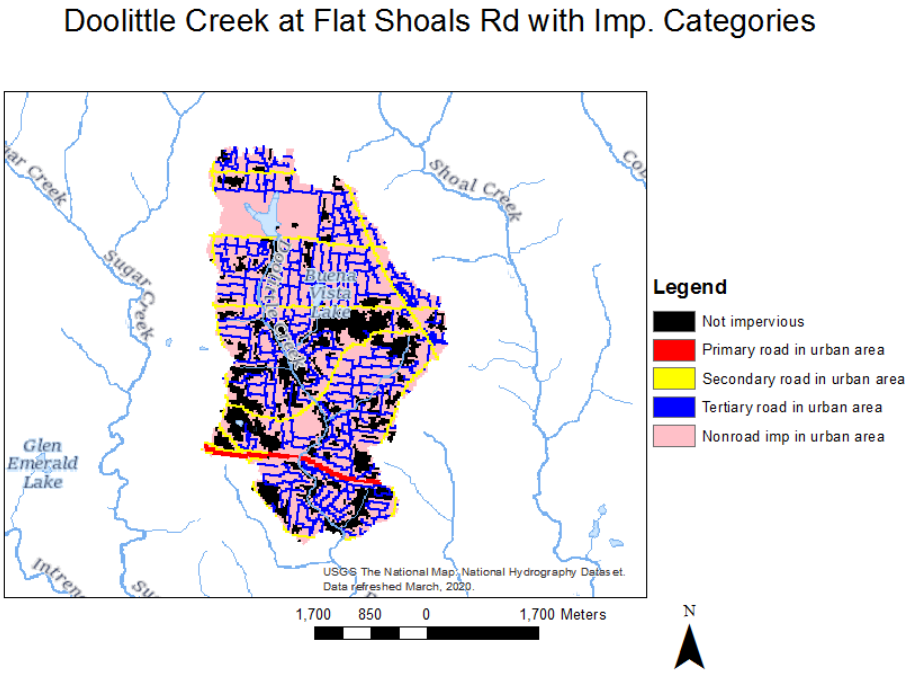

Figure 4: Outline of the drainage area for Doolittle Creek at Flat Shoals Road. Legend shows impervious land use descriptors per MRLC NLCD.

Table 1: Summary information for the 3 USGS gages used as storm sampling sites and their associated drainage areas.

USGS Gage ID	02203700	02203831	02203900
Stream name and nearest cross-streets	Intrenchment Creek at Constitution Rd	Doolittle Creek at Flat Shoals Rd	South River at Flakes Mill Rd
Coordinates	33.6888889, -84.330556	33.705556, -84.292500	33.665637, -84.224429
Drainage area (km^2)	27.5	11.01	256.4
Percent ISC	81.42	79.20	73.68

Table 2: Areal land use categories for the 3 gages used in this study. SR at Flakes Mills is the most downstream site sampled, representing the land use for the entire watershed.

Land Use	SR at Flakes Mill Rd	Doolittle at Flat Shoals Rd	Intrenchment at Constitution Rd
Developed, Open	26.9	41.7	21.3
Developed, Low	27	27.4	29.7
Developed, Medium	11.4	6.4	17.6
Developed, High	8.3	3.7	12.8
Deciduous Forest	9.7	5.4	7
Evergreen Forest	8.3	9.8	3.4
Mixed Forest	3.8	4.1	4
Other	4.4	1.6	4.2
Total Urban	73.6	79.2	81.4
Total Forest	21.9	15.4	14.4

Table 3:Types of imperviousness present in SRW by areal percentage, as calculated for the entire watershed.

Impervious Types in SRW	Percentage of Total Area
Not impervious	26.3
Primary road in urban area	1.8
Secondary road in urban area	5.4
Tertiary road in urban area	20.03
Nonroad imp in urban area	46.5

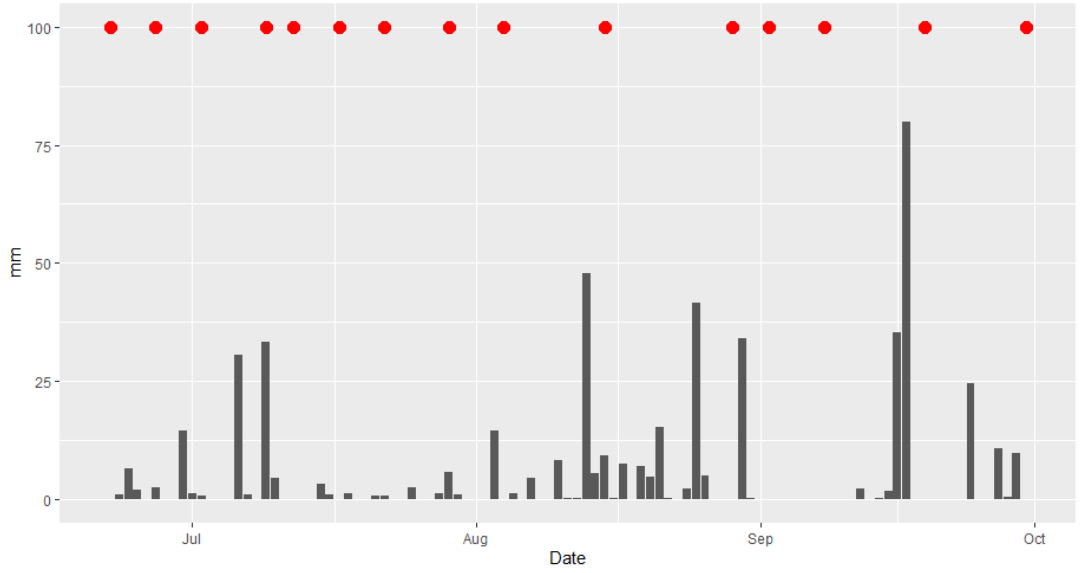

Figure 5: Hyetograph for summer 2020, South River at Flakes Mill Road (USGS 02203900). Red dots represent baseflow sampling dates.

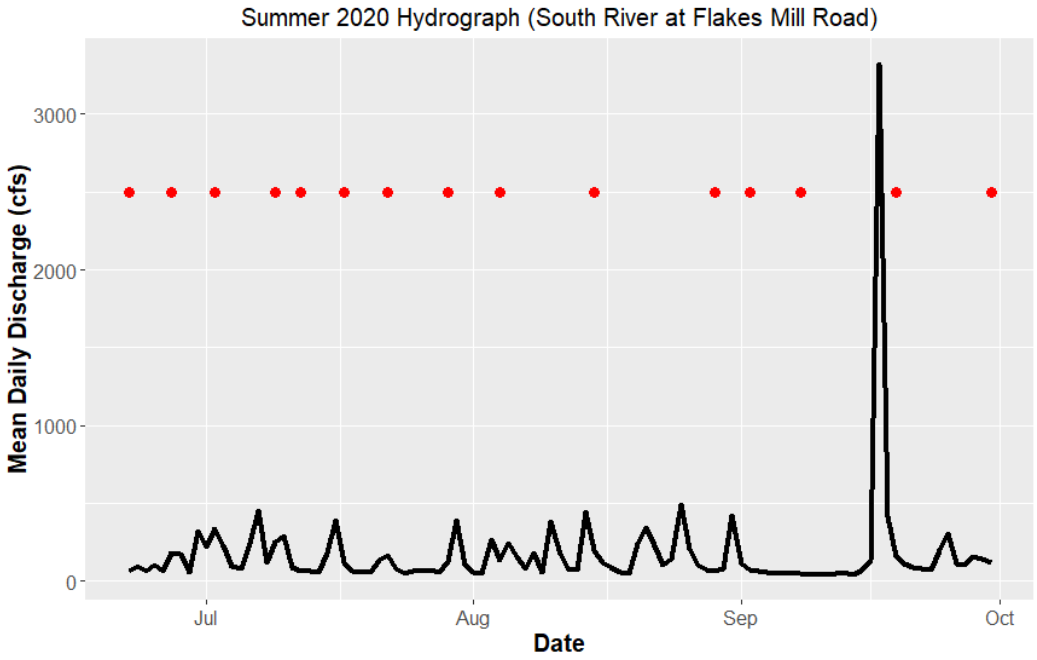

Figure 6: Hydrograph for Summer 2020, South River at Flakes Mill Road (USGS 02203700). Red dots represent baseflow sampling dates.

2.3 Surface water sampling

Regular baseflow sampling was performed from June through September 2020 (Fig. 5; Fig. 6). Water quality samples were collected approximately weekly, for a total of 15 times from a total of 18 sites (Fig. 1) in the South River Watershed (total baseflow samples collected = 270). Of the 18 sites, three were collocated with the USGS stream gages discussed in section 2.3. These 18 baseflow sampling sites were selected in an attempt to adequately characterize the headwaters of the South River Watershed (i.e., locations representative of the most upstream reaches of first-order tributaries in the basin). However, due to site access limitations, sample sites were ultimately placed at the most proximal public cross-street to the actual headwater locations. Samples were collected from each site using two 60 mL HDPE bottles (as well as one duplicate per sample set) and rinsed three times with stream water prior to collection. Samples were filtered using Millipore brand, 0.45 µm pore size paper filters and stored at 4°C prior to analysis.

In addition to baseflow sampling, storm event sampling was performed during summer 2020. Time-series concentrations were quantified at the three USGS gages (Fig. 7) for 13 discrete storm events from June through September 2020. Temporal resolution varied between storms due to equipment limitations. When possible, samples were collected hourly with an ISCO, and additional grab samples were collected at finer temporal intervals when peak discharge was during the day. Through the selection of USGS gages as sample points, 15-minute discharge and SPC measurements were also available for use in C-Q analysis.

2.4 Hydrochemical analyses

Field parameters were measured and recorded *in-situ* at each baseflow sample site. Time, temperature (C°), barometric pressure (mm Hg), DO (% saturation and ppm), SPC (µS/cm), and

pH were measured using a YSI brand Pro DDS handheld probe that was calibrated in the lab before use. Baseflow samples were analyzed for major ion concentrations (Ca^{2+}, Mg^{2+}, Na^{+}, K^{+}, Cl^{-}, SO_4^{2-}, F^{-}, Br^{-}, and NO_3^{-}) using a ThermoScientific brand Aquion Ion Chromatograph at the Ledford Urban Hydrology Lab (Georgia State University). The Aquion Ion Chromatograph uses 5 in-house cation calibration standards and 5 in-house anion calibration standards for QA/QC in addition to running external USGS standards for calibration checks. Storm event analyses were identical to those described for baseflow, with the omission of the measurement of *in-situ* field parameters.

2.5 C-Q analysis

After sample collection and chemical analysis, C-Q "hysteresis loops" were generated for all solutes at each of the gages and rotational direction was determined. To make more robust comparisons between and among gages, events, and solutes, a normalized hysteresis index (HI) was calculated using methodology from Lloyd et al. (2016). To calculate HI, discharge (Q) and concentration (C) must first be normalized to a 0-1 scale, as in the following equations:

$$\text{Normalized C} = \frac{C_i - C_{min}}{C_{max} - C_{min}} \quad (1)$$

$$\text{Normalized Q} = \frac{(Q_i - Q_{min})}{Q_{max} - Q_{min}} \quad (2)$$

Where C_i and Q_i are values at given timestep (i), C_{max} and Q_{max} are maximum values for a given storm event, and C_{min} and Q_{min} are minimum values for a given storm event.

After normalization, the HI is calculated by subtracting concentration values on the falling limb of the hydrograph at a given discharge from those on the rising limb at the same discharge value:

$$HI = C_{RL\_norm} - C_{FL\_norm} \quad (3)$$

Where C_{RL_norm} represents a rising limb concentration at a given discharge value, and C_{FL_norm} represents a falling limb concentration at a given discharge value. As such, values of the HI will fall between -1 and 1. Positive values represent clockwise rotation, and negative values represent counterclockwise rotation. The magnitude of the value represents the size of the area inside the loop, which is representative of the relative magnitude of the hysteretic response. Another advantage of this index is that it can be calculated at different levels of resolution (i.e., the user can choose to calculate the HI at any increment of discharge). For this study, a script was executed in R that calculated the HI at 2% increments of discharge, giving 50 discrete HI values that were averaged to yield the final value (Lloyd et al., 2016; Vaughan et al., 2017; Marsh and Moore, 2020).

In addition to HI, a normalized flushing index (FI) was calculated according to methodology from Vaughan et al. (2017):

$$FI = C_{Qpeak\_norm} - C_{Qinitial\_norm} \quad (4)$$

Where C_{Qpeak_norm} represents the normalized concentration at peak discharge, and $C_{Qinitial\_norm}$ represents the initial normalized concentration for the storm event. As such, values of the FI also fell between -1 and 1. Positive values represent a flushing or "transport-limited" response for a particular solute, whereas negative values represent a dilution or "source-limited" response (Koenig et al., 2017). Moreover, like the HI, the magnitude of the FI value represents the relative magnitude of the flushing/dilution response. Plots of HI vs. FI for each storm show the individual behavior and allow for inter-storm and inter-site comparison (Fig. 7; Vaughan et al., 2017). Using these two indices and plotting the results provided a robust method to compare C-Q responses among and between storms, sites, and solutes, thereby more easily parsing mobilization/transport mechanisms and processes for various solutes on the watershed scale.

(Aguilera and Melack, 2018; Marsh et al., 2018; Lloyd et al., 2016). Finally, we considered the nature of longer-term C-Q relationships at each of the three study gages by producing plots of 15-minute discharge and concentration measurements for the entire period of baseflow sampling (n = 9696). The characteristics of C-Q relationship in these datasets were examined.

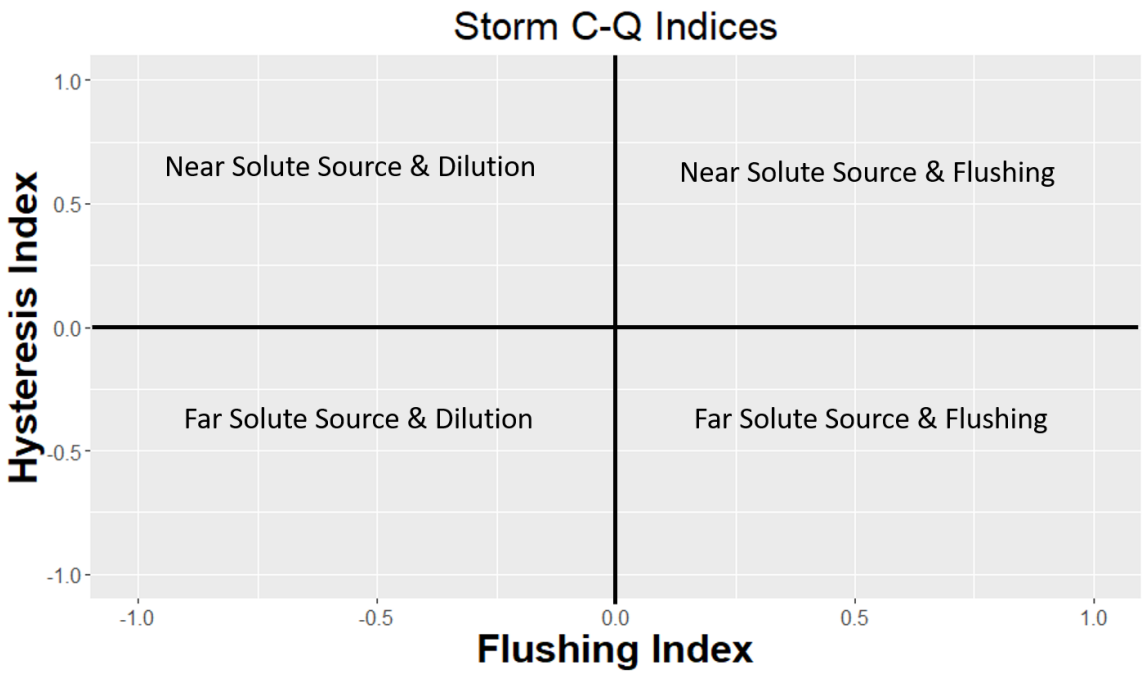

Figure 7: Conceptual diagram of storm response indices, with classifications labeled for their associated quadrants.

2.6 LULC data and analysis

2.6.1 Land use and land cover (LULC) analysis

In addition to discharge data, solute concentrations, and field parameters, supplementary data were obtained and consolidated for analysis. Geospatial data were acquired from USGS and the Multi-resolution Land Characteristics Consortium (MRLC), in conjunction with analyses in ArcGIS (ESRI, 2020). The percentage of various land cover classes, per the MRLC 2016

National Land Cover Database (NLCD), was calculated using ArcMap (ESRI, 2020) for the catchments draining each gage. The NLCD is a comprehensive raster dataset of land use in the contiguous US, developed by a consortium of federal agencies. This 30m-resolution raster was last updated in 2016 and uses a 16-class legend for land use designation. Additionally, the same percentage calculation procedure was repeated using the NLCD 2016 Developed Urban Imperviousness Descriptor raster to quantify areal percentages of various types of impervious surfaces, including primary and secondary roads. Finally, 25m buffers were constructed around polylines representing the stream itself. The percentage of land use according to the NLCD was then calculated the area enclosed by the buffer. Linear regression was performed to test the significance of correlation between land use and land cover on baseflow water quality and the significance of the linear regressions was test with the lm function in R which uses ANOVA to test for significance. In addition to land use percentages we also found total forested and total urban percentages based on the NLCD classification.

2.6.2 Principal component analysis (PCA)

Principal component analysis (PCA) was also performed to reduce the dimensionality of the baseflow data set by forming linear combinations of potential explanatory variables from 11 original variables measured at baseflow (Ca^{2+}, Mg^{2+}, Na^{+}, K^{+}, Cl^{-}, SO_4^{2-}, and NO_3^{-}, temperature, dissolved oxygen using % saturation, pH, and SPC). The use of PCA is popular with multivariate, environmental data sets. PCA can parse driving trends in a dataset, as well as more clearly show groupings of observations with similar combined characteristics (i.e., principal components). This technique has been applied widely in hydrology, including with

hydrochemical (Lautz and Fannelli, 2008), hydromorphic (Singh et al., 2008), and hydrometeorological (Shaharudin et al., 2018) data sets. The analysis was performed by using the prcomp function in base R (R Core Team, 2020), in conjunction with the ggplot2 package (Wickham, 2020) to plot resulting principal components scores for each observation.

3 RESULTS

3.1 Baseflow

3.1.1 Hydrochemistry

Baseflow concentrations across the South River were largely consistent at each site over the summer (Fig. 8 and Fig. 9 show NO_3^- and Cl^-, with similar patterns for other ions), with median NO_3^- concentrations between 0.5 and 1 mg N/L and Cl^- between 4 and 8 mg/L. This discussion focuses on patterns in biogeochemically-available NO_3^- and conservative Cl^- to separate conservative vs. non-conservative behaviors. For NO_3^-, there are a few outlier sites that show greater temporal variation (Fig 8). Four of the 18 sampling sites show median values below 0.5 mg N/L. Of those sites, BS-12 and BS-16 are proximally located, and they represent the outlet and inflow for a small pond. These sites also share a relatively small drainage area (5.9 km^2 for BS-12 and 5.7 km^2 for BS-16), as well as relatively low urban land use percentages (60.0% for BS-12 and 59.3% for BS-16) compared to other sample locations. The other two sites that exhibited relatively low (below 0.5 mg N/L) median NO_3^- concentrations were BS-2 and BS-7. BS-2 (Conley Creek at River Road) is associated with a fairly low drainage area (14.4 km^2) and exhibits the smallest percentage of developed (urban) land use of all drainage areas in the study at 43.6%. BS-7 (unnamed tributary to Cobbs Creek at Cocklebur Trail) is also notable in that it is associated with the smallest drainage area (0.6 km^2) of all sites studied. However, the drainage area associated with this site also exhibits the highest areal urban land use percentage of all studied sites (87.1%). Spatial and temporal variability of Cl^- concentrations at baseflow largely mirrored that of the NO_3^- concentrations discussed above. As with NO_3^- concentrations, the two sites associated with the small pond (BS-12 and BS-16) have median Cl^- concentrations below 4 mg/L (Fig. 9). Additionally, BS-18 represents the highest median Cl^- site with the

highest temporal variability. Unlike with NO_3^-, BS-2 and BS-7 did not exhibit lower (below 4 mg/L) Cl^- concentrations.

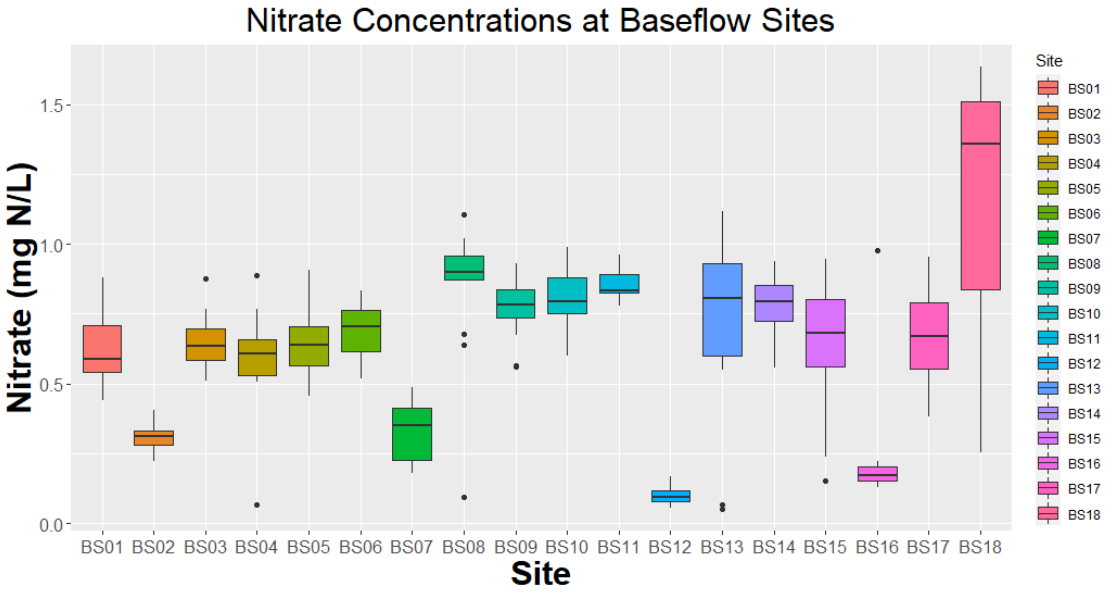

Figure 8: Boxplot of N concentrations in mg N/L at each baseflow sampling site. The median is shown with the solid line while the box covers the 25th to 75th percentiles. Vertical lines show the 5th to 95th percentiles and outliers area shown with dots.

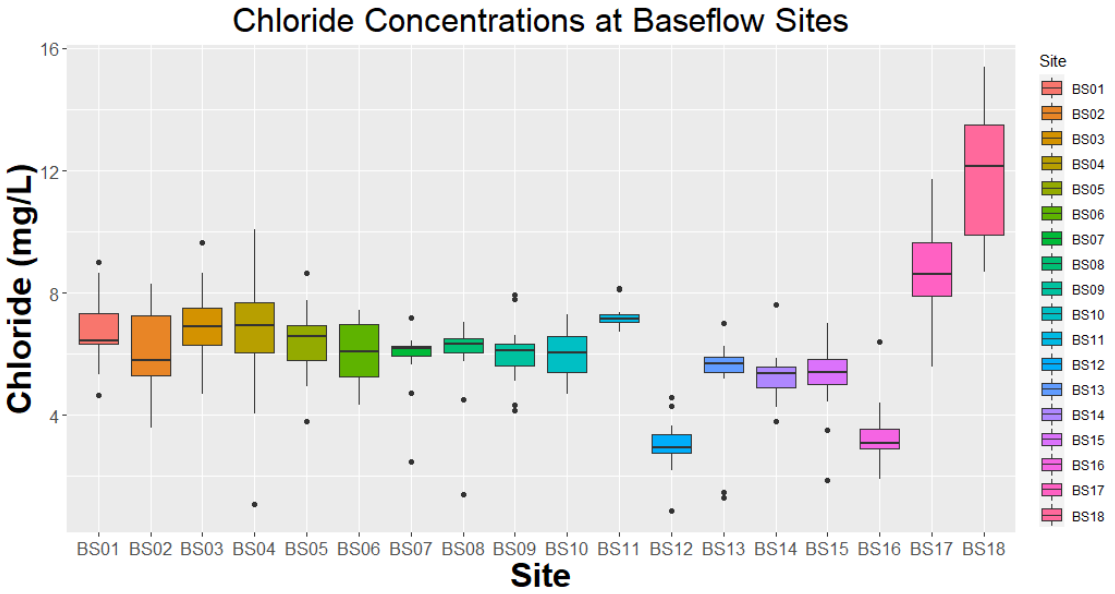

Figure 9: Boxplot of Cl concentrations in mg/L at each baseflow sampling site. The median is shown with the solid line while the box covers the 25th to 75th percentiles. Vertical lines show the 5th to 95th percentiles and outliers area shown with dots.

Comparing Cl^- to NO_3^- concentrations for all baseflow samples shows the non-conservative behavior of NO_3^-, (Fig. 10), especially when compared to the conservative behavior of both Na^+ and Cl^- (Fig. 11). The more scattered relationship between NO_3^- and Cl^- suggests that that concentrations are being affected by site-specific in-stream processes such as nitrification, denitrification, assimilation, and mineralization.

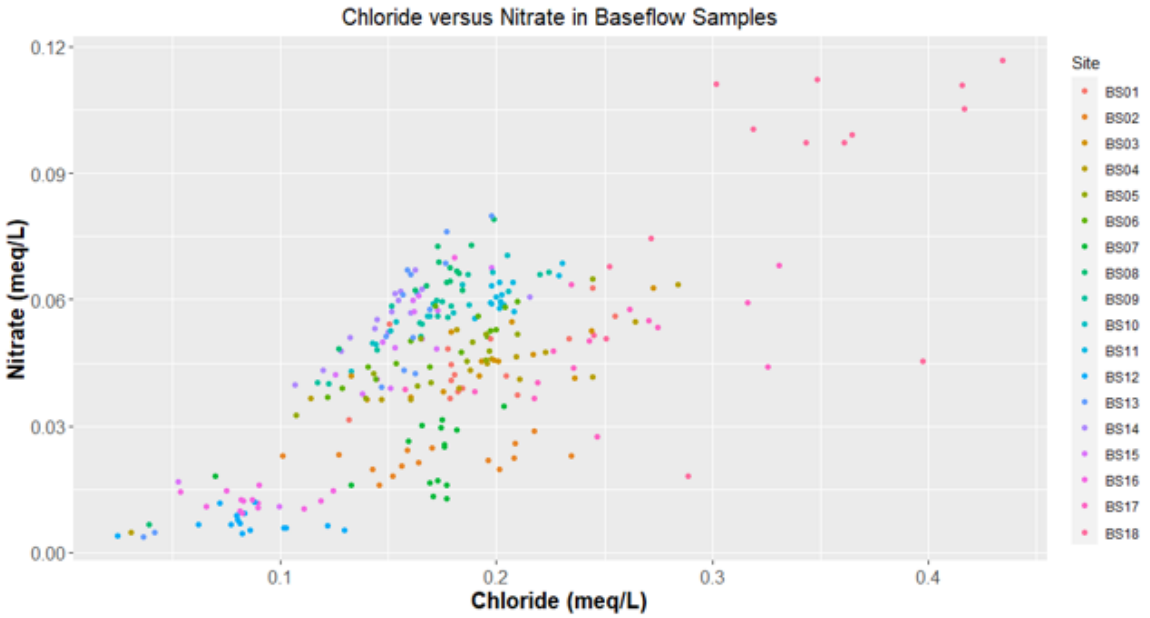

Figure 10: Scatterplot showing Cl^- versus NO_3^- concentrations. Dots are colored by site.

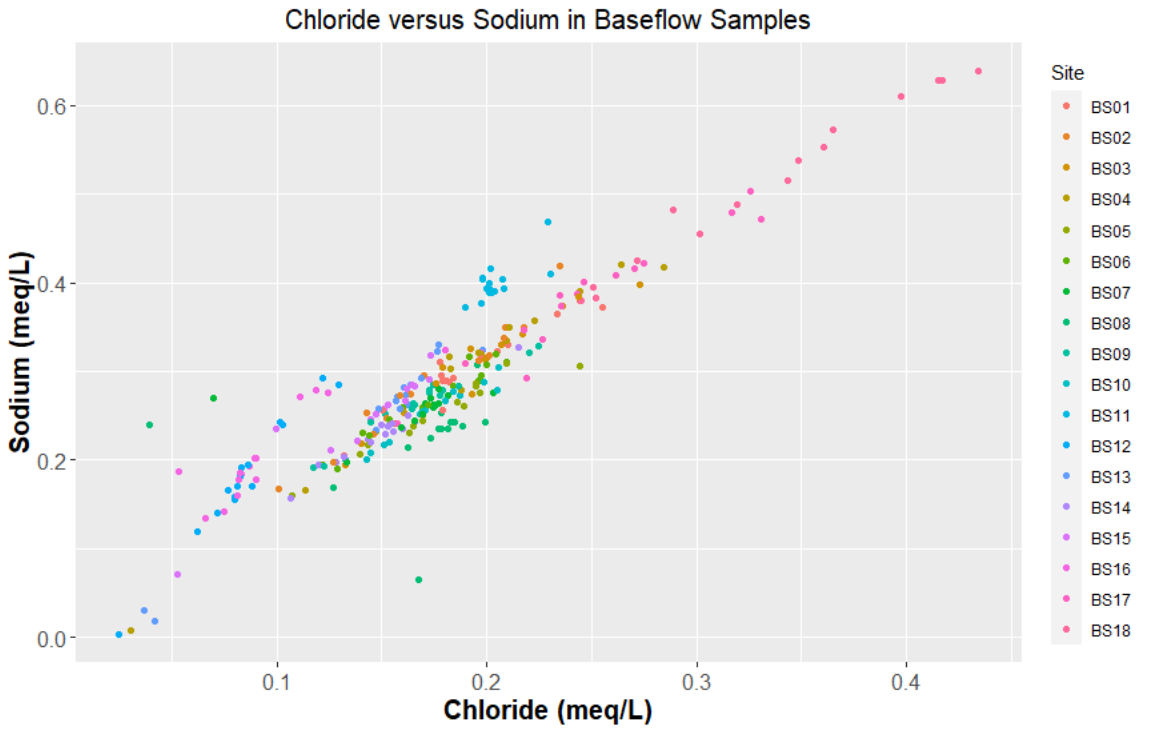

Figure 11: Scatterplot showing Cl^- versus Na^+ concentrations. Dots are colored by site.

BS-18 exhibited by far the most variation of the baseflow sites sampled (Figs. 8 and 9). Representing one of the three USGS gage sites used in the study (USGS 02203700), BS-18 is located approximately two miles downstream from the Custer Avenue and East Area combined sewer overflow (CSO) facilities (City of Atlanta, 2020). The Custer Avenue facility was built as an emergency treatment plant to limit CSO bypasses of wastewater treatment plants (City of Altana, 2005). During light rainfall events, such facilities are typically not used. In 2019 the Custer Ave facility was associated with 3 discharge events, while the East Area Intrenchment Creek Overflow was associated with 38 discharge events. Notably, the Custer Street facility released overflow at rainfall events as low as 0.25 inches in that year (City of Atlanta, 2019). When rainfall causes overflows, the Custer Street facility is meant to "capture, treat and disinfect" the combined sewer overflows (City of Atlanta, 2005). Characteristic baseflow hydrographs from the site (Fig. 12) suggest that periodic release events occur originating from

the upstream CSO facility, where baseflow is elevated and sustained for relatively long periods, creating a plateau-shaped hydrograph. These releases are thought to follow relatively large storm events. Indeed, the suspected CSO release events that we sampled (Fig. 12) occurred approximately 12 hours after a relatively large storm event in the area. Unexpectedly, Cl^- and NO_3^- show divergent responses to rising discharge from the suspected event.

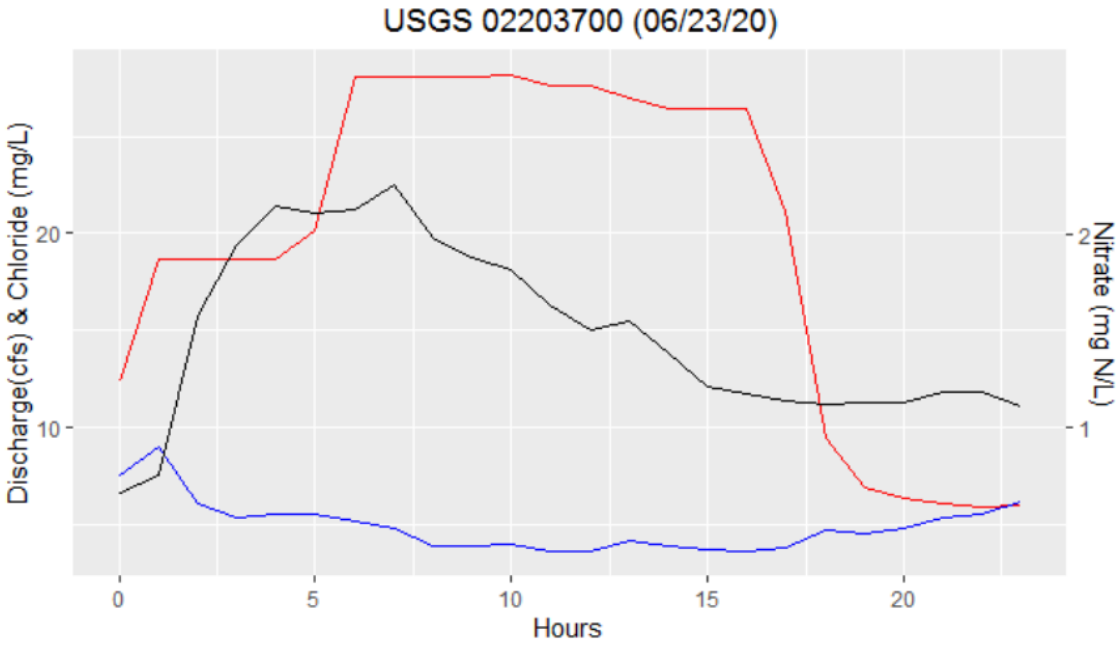

Figure 12: Time-series plot of Cl^-, NO_3^-, and 15-minute discharge measurement for suspected CSO outfall event at USGS 02203700, 06/23/20). Discharge in red, Cl^- in black, and NO_3^- in blue.

3.1.2 Influence of urban land use on baseflow water quality

Examination of the land use data set reveals a few general characteristics. The most apparent characteristic is that this is all of the sampling sites are associated with drainage areas with relatively large proportions of ISC. Total developed (urban) land use ranged from 43.6% (BS-2) to 87.1% (BS-7). Testing for correlations between total urban/forested land use and mean baseflow solute concentrations (Table 4), we found a significant positive relationship between

mean NO_3^- concentration in baseflow and total urban land use as a percent ($p = 0.013$, Fig. 13) and a negative relationship between mean NO_3^- and total forest as a percent ($p = 0.014$, Fig. 14). We also found a significant ($p = 0.015$) negative relationship between mean Cl^- and forested land use as a percent among all watersheds ($p = 0.015$, Fig. 15). The relationship between Na^+ and total forest was also negative and was marginally significant ($p = 0.064$).

Table 4: Summary of the linear regressions performed between LULC and hydrochemical data. Values include the slope of the relationship, the R-squared value, and the p-value. P-values lower than 0.05 are in bold.

Comparison	p-value	R^2	Slope
Mean NO3 to Total Urban	**0.013**	0.33	0.0143
Mean NO3 to Total Forest	**0.014**	0.32	-0.0128
Mean Na to Total Urban	0.33	0.059	0.0427
Mean Na to Total Forest	0.064	0.198	-0.119
Mean SO4 to Total Urban	0.79	0.0047	0.0269
Mean SO4 to Total Forest	0.26	0.0777	-0.1678
Mean Cl to Total Urban	0.108	0.15	0.073
Mean Cl to Total Forest	**0.015**	0.3144	-0.2445
Mean K to Total Urban	0.805	0.0039	0.0033
Mean K to Total Forest	0.171	0.1136	-0.0269
Mean Ca to Total Urban	0.623	0.0155	-0.374
Mean Ca to Total Forest	0.872	0.0017	-0.0187

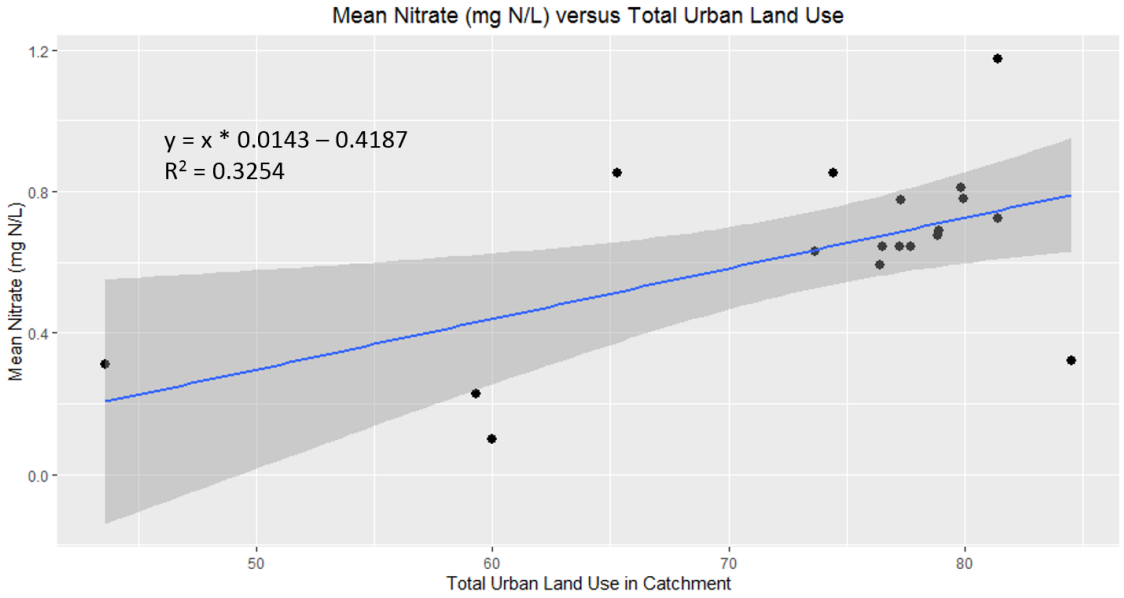

Figure 13:Scatterplot showing mean baseflow concentrations observed on the y-axis and total urban land use (as a percent) for each watershed on the x-axis.

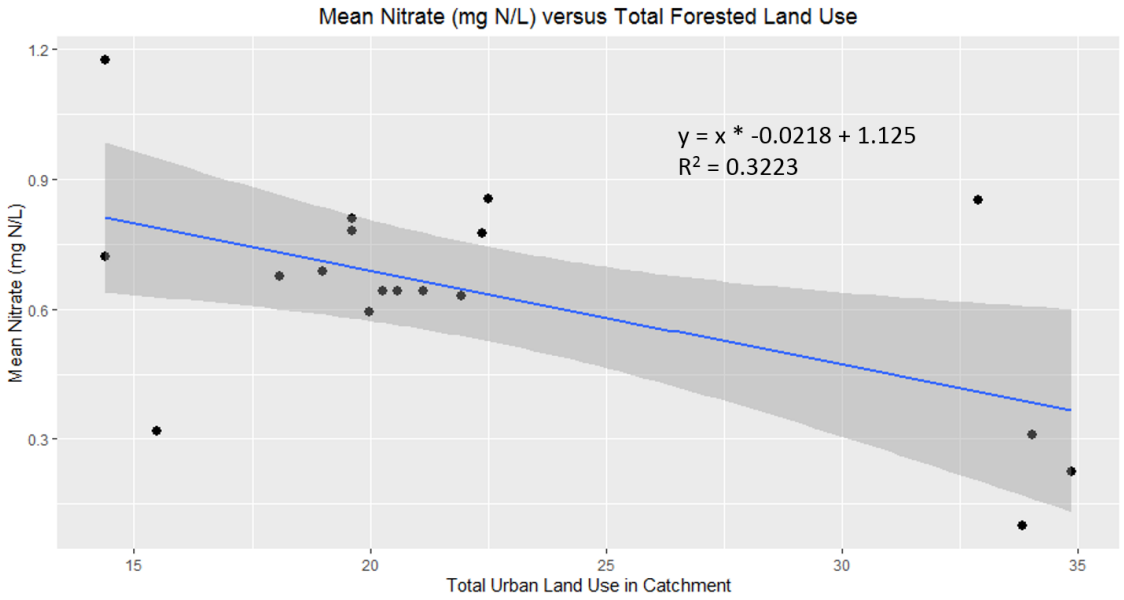

Figure 14: Scatterplot showing mean baseflow N concentrations on the y-axis, and total forested land use on the x-axis.

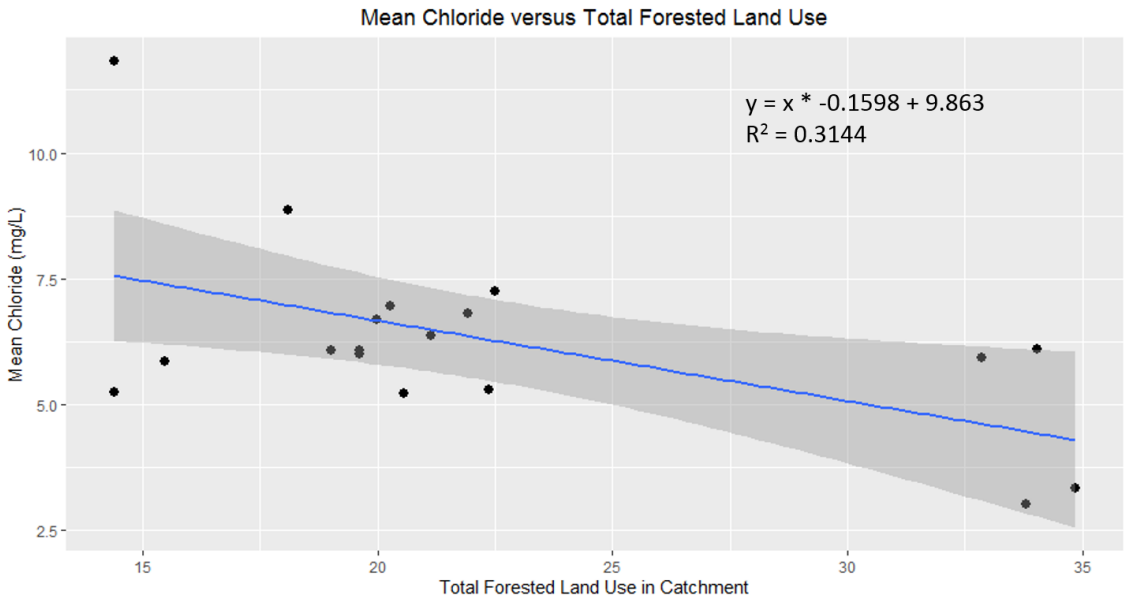

Figure 15: Scatterplot showing mean baseflow Cl concentrations on the y-axis, and total forested land use on the x-axis.

Performing the same areal percentage calculations, but instead using a 25m buffer around the stream itself as opposed to the entire watershed, yielded somewhat similar results in terms of the significance of linear regressions (Table 5). As with the overall land use percentage value, we found a significant relationship between mean NO_3^- values and percent urban land use for a given site using the 25m buffer (p=0.028). However, this is the only relationship that held, suggesting that for this system, total watershed land use is a more accurate indicator of water quality.

Table 5:Summary of the linear regressions performed between LULC (for a 25m buffer around the stream contributing to discharge at each site) and hydrochemical data. Values

include the slope of the relationship, the R-squared value, and the p-value. P-values lower than 0.05 are in bold.

Comparison	p-value	R^2	Slope
Mean NO3 to Total Urban	**0.028**	0.267	0.028
Mean NO3 to Total Forest	0.175	0.112	-0.008
Mean Na to Total Urban	0.840	0.003	0.005
Mean Na to Total Forest	0.689	0.010	-0.016
Mean SO4 to Total Urban	0.740	0.007	-0.020
Mean SO4 to Total Forest	0.760	0.006	-0.028
Mean Cl to Total Urban	0.323	0.061	0.028
Mean Cl to Total Forest	0.311	0.064	-0.043
Mean K to Total Urban	0.683	0.011	-0.003
Mean K to Total Forest	0.728	0.008	-0.004
Mean Ca to Total Urban	0.213	0.095	-0.056
Mean Ca to Total Forest	0.609	0.017	0.035

3.1.3 Principal component analysis

Results of the PCA showed a clear distinction between the first three principal components that were generated, with PC1 explaining 45.0% of the variance, PC2 explaining 17.7%, and PC3 explaining 11.5% (Table 6). PC1 had a strong negative loading for Na^+, SO_4^{2-}, Cl^-, Ca^{2+}, and SPC, which we interpret as a groundwater signal, while PC2 had a strong positive loading for NO_3^- and DO and a negative loading for temperature and Mg^{2+}, which we interpret as an in-stream metabolism signal (Fig. 16). PC3 had a strong positive loading for temperature and K^+ and a strong negative loading for pH, which we believe represents antecedent moisture conditions (Table 7). Furthermore, plotting PC1 versus PC2 and PC2 versus PC3 scores for each sample and overlaying ellipses representing sample site groupings further underscores the contrast between groundwater-driven and metabolism-driven sites, as well as the level of variability observed in component scores observed at each site (Fig. 17; Fig. 18).

Table 6: The standard deviation of each component, the proportion of variance accounted for by each component, and the cumulative (total) proportion of variance explained by each component and the others that preceded it. Shown for first 3 principal components.

Component	PC1	PC2	PC3
Standard Dev	2.2237	1.3936	1.1243
Proportion of Variance	0.4495	0.1766	0.1149
Cumulative Proportion	0.4495	0.6261	0.7410

Table 7: Coefficients (loadings) used in the calculation of principal component scores for each observation. The highest loadings for each PC are bolded.

Component	PC1	PC2	PC3
Chloride	**-0.400**	0.220	-0.019
Nitrate	-0.260	**0.450**	-0.053
Sulfate	**-0.400**	-0.003	0.094
Sodium	**-0.426**	0.055	-0.03
Potassium	-0.350	0.022	**0.368**
Magnesium	-0.150	**-0.590**	-0.165
Calcium	**-0.370**	-0.320	0.081
Temp	0.069	**-0.317**	**0.523**
DO	-0.095	**0.363**	0.298
pH	-0.092	0.066	**-0.645**
SPC	**-0.350**	-0.253	-0.202

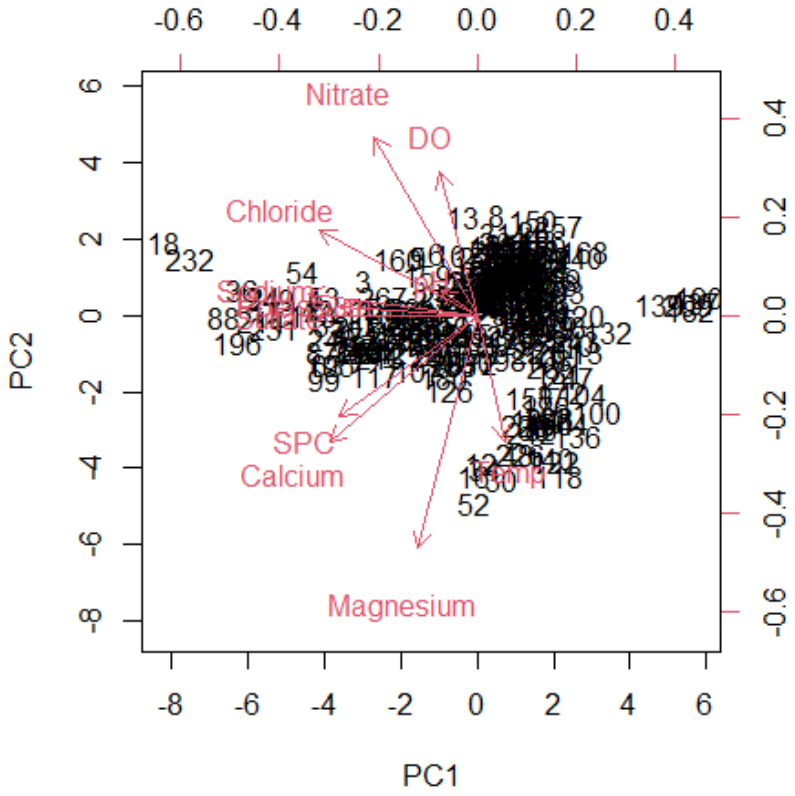

Figure 16: Biplot of PC1 and PC2 values for each observation (numbered), as well as the magnitude and direction associated with the eigenvector generated for each variable.

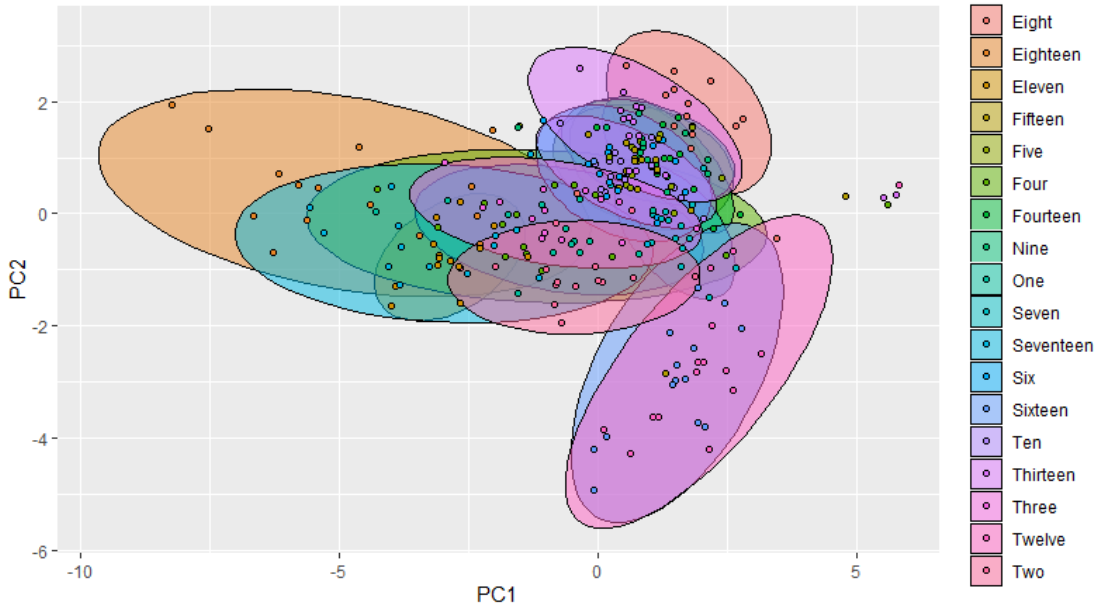

Figure 17: Result of principal component analysis of baseflow sampling data. PC1 is plotted on x-axis and PC2 is plotted on y-axis. 95% confidence ellipses were drawn around samples from each site.

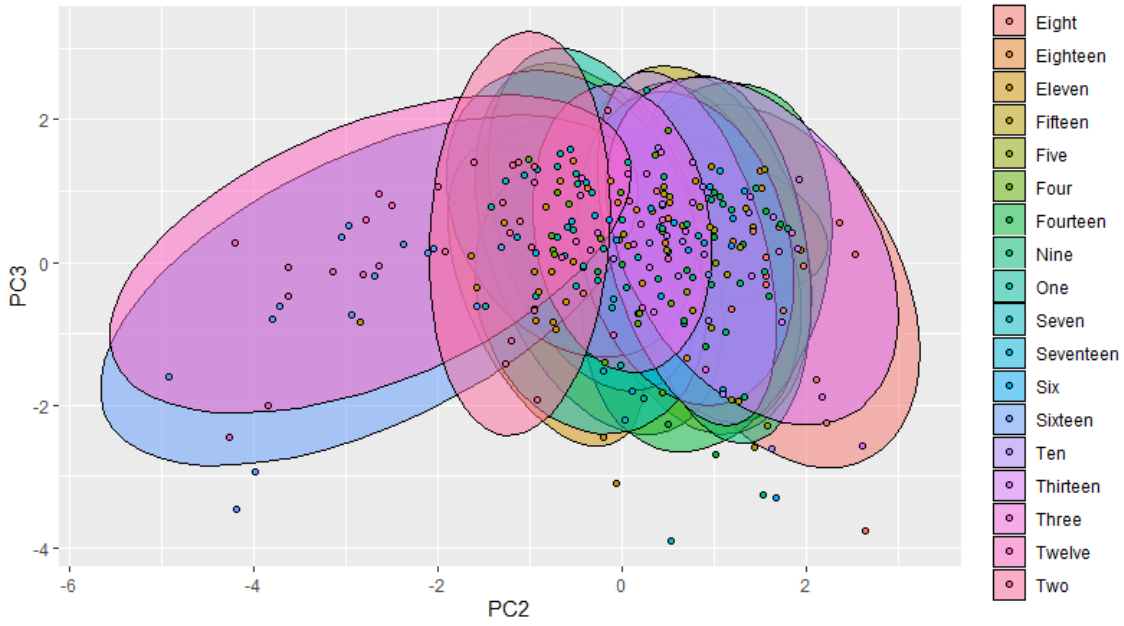

Figure 18: Result of principal component analysis of baseflow sampling data. PC2 is plotted on x-axis and PC3 is plotted on y-axis. 95% confidence ellipses were drawn around samples from each site.

3.2 Stormflow

3.2.1 Hysteresis loop shape and direction

Thirteen discrete storm events were sampled among the 3 gages from June through August 2020, and their general event-scale C-Q characteristics with respect to SPC, Cl^- and NO_3^- are listed in Table 8. Overall, loops exhibited exclusively clockwise or complex rotation and almost exclusively dilutive slopes (see representative examples in Fig. 19, Fig. 20, Fig. 21, and Fig. 22). The only flushing response was seen for NO_3^- on 3 instances (see Fig. 23 for example).

Table 8: Summary of storm responses. DOOL refers to Doolittle Creek at Flat Shoals Road (USGS 02203831); INT refers to Intrenchment Creek at Constitution Road (USGS 02203700); SR refers to South River at Flakes Mill Road (USGS 0220900).

Storm ID	NO3 Response	NO3 Rotation	Cl Response	Cl Rotation	SPC Response	SPC Rotation
DOOL_072520	flushing	clockwise	dilution	clockwise	dilution	clockwise
DOOL_073020	dilution	complex	dilution	complex	dilution	complex
DOOL_080320	dilution	clockwise	dilution	clockwise	dilution	clockwise
DOOL_080520	dilution	complex	dilution	complex	dilution	complex
DOOL_082120	dilution	complex	dilution	complex	dilution	complex
INT_063020	dilution	clockwise	dilution	clockwise	dilution	clockwise
INT_070220	flushing	clockwise	dilution	clockwise	dilution	clockwise
INT_080320	dilution	clockwise	dilution	clockwise	dilution	clockwise
INT_082120	dilution	complex	dilution	complex	dilution	complex
INT_082420	dilution	complex	dilution	complex	dilution	complex
SR_070620	dilution	clockwise	dilution	clockwise	dilution	clockwise
SR_072120	dilution	clockwise	dilution	clockwise	dilution	clockwise
SR_072520	flushing	clockwise	dilution	complex	dilution	complex

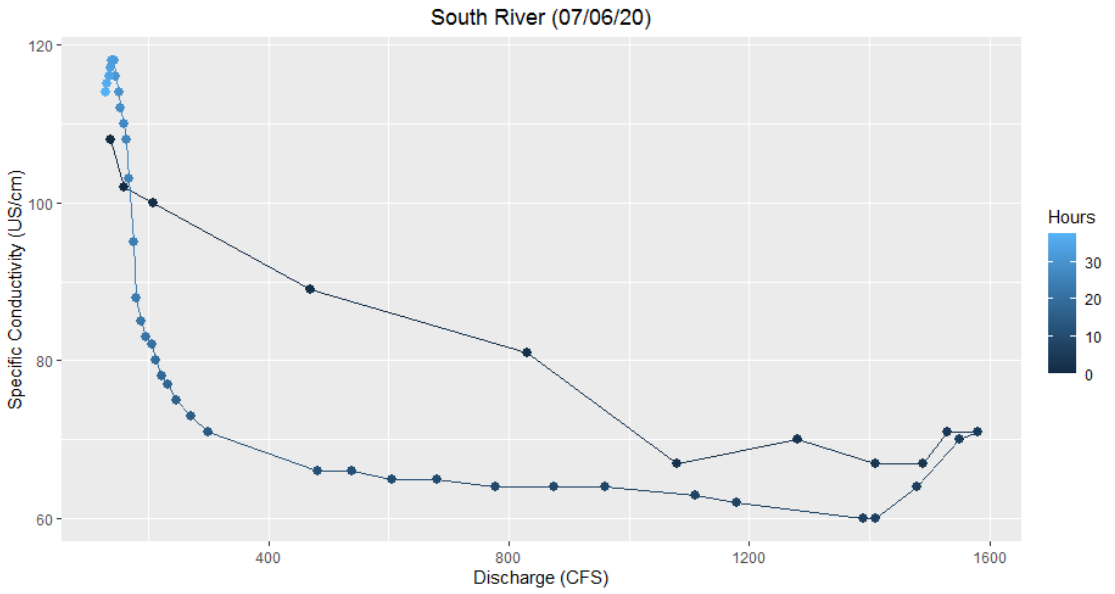

Figure 19: C-Q plot (SPC) for South River (07/06/20).

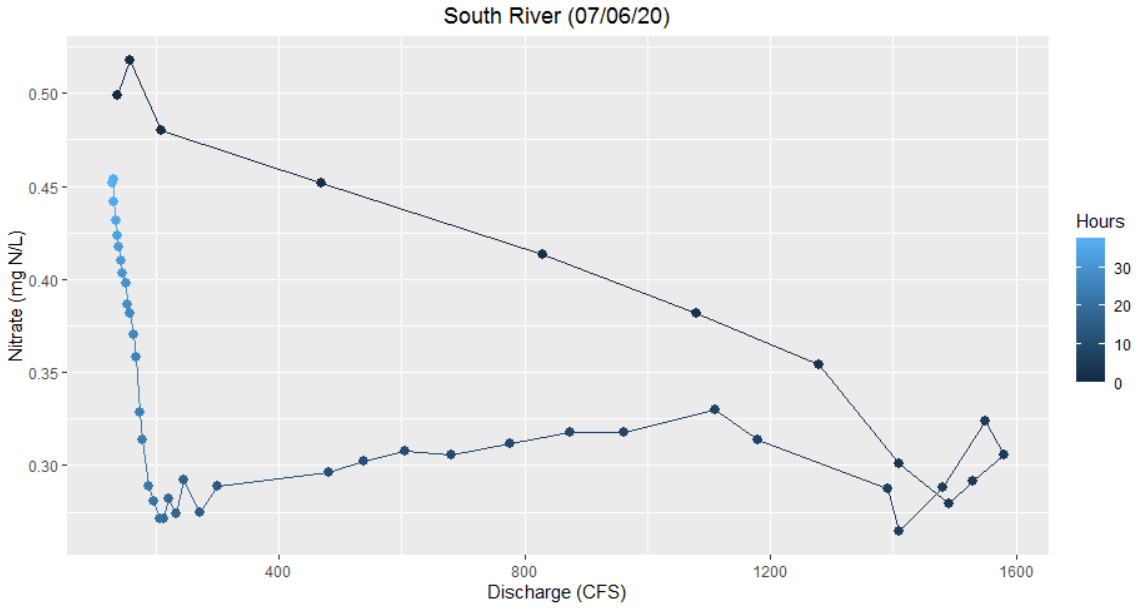

Figure 20: C-Q plot (Nitrate) for South River (07/06/20).

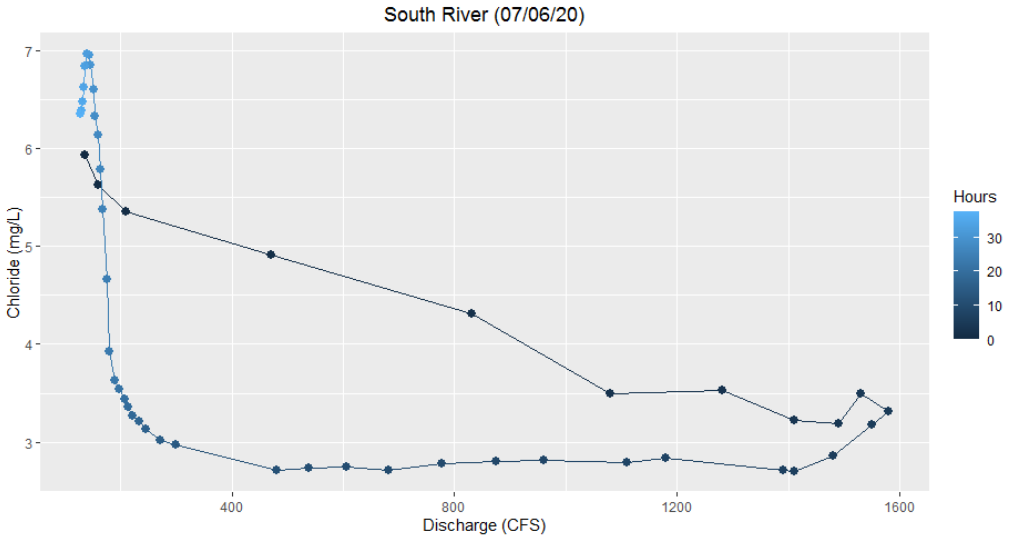

Figure 21: C-Q plot (Chloride) for South River (07/06/20).

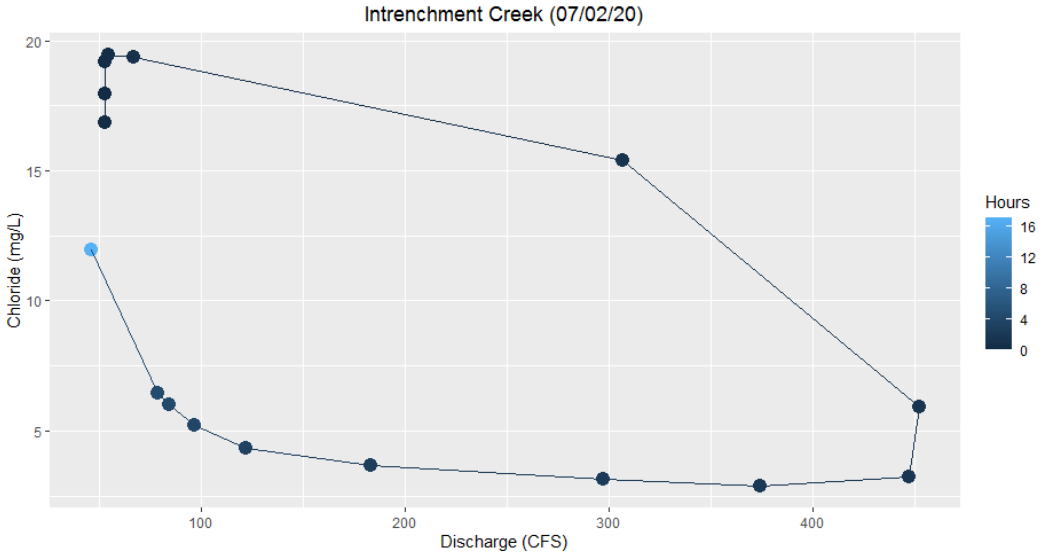

Figure 22: C-Q plot (Chloride) for Intrenchment Creek (07/02/20)

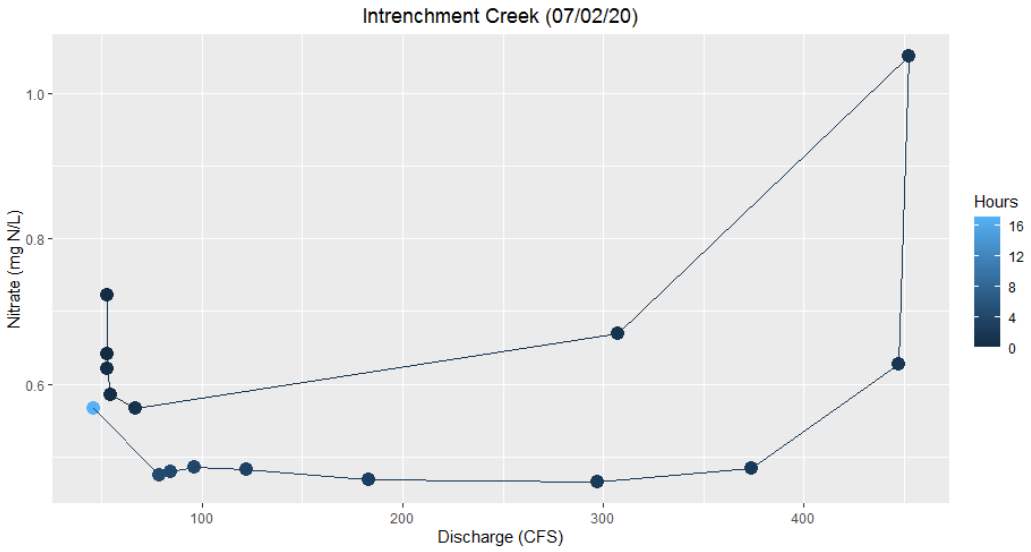

Figure 23: C-Q plot (Nitrate) for Intrenchment Creek (07/02/20). Note anomalous flushing response.

3.2.2 Flushing index (FI) & Hysteresis index (HI)

The response for NO_3^- for the three storms which exhibited flushing (Doolittle 07/25/21, Intrenchment 07/02/21, and Intrenchment 08/24/21) is shown by plotting FI against HI (Fig. 24). Storms with a dilutive signal had a negative FI of relatively large absolute value, showing dilution was over 50% for most of the storms. The clockwise rotation seen during most storms is represented by the positive HI, with the few complex storms having a negative HI. There is no clear pattern between NO_3^- C-Q behavior and antecedent moisture conditions, although the storm with the greatest flush did have the greatest antecedent moisture conditions (Fig. 25).

Unlike with NO_3^-, there were no storms in the study which exhibited flushing for Cl^- (Fig. 26). Although every storm was dilutive in terms of Cl^-, the storm event that was closest to flushing response had a very low value for antecedent precipitation (Fig. 27). Additionally, as with NO_3^-, most storms exhibited a relatively high (over 50%) dilution response for Cl^-. Positive

hysteresis indices for all storms show that all loops generated for Cl^- were predominantly clockwise, indicating a proximal or geogenic solute source diluted by an influx of event water.

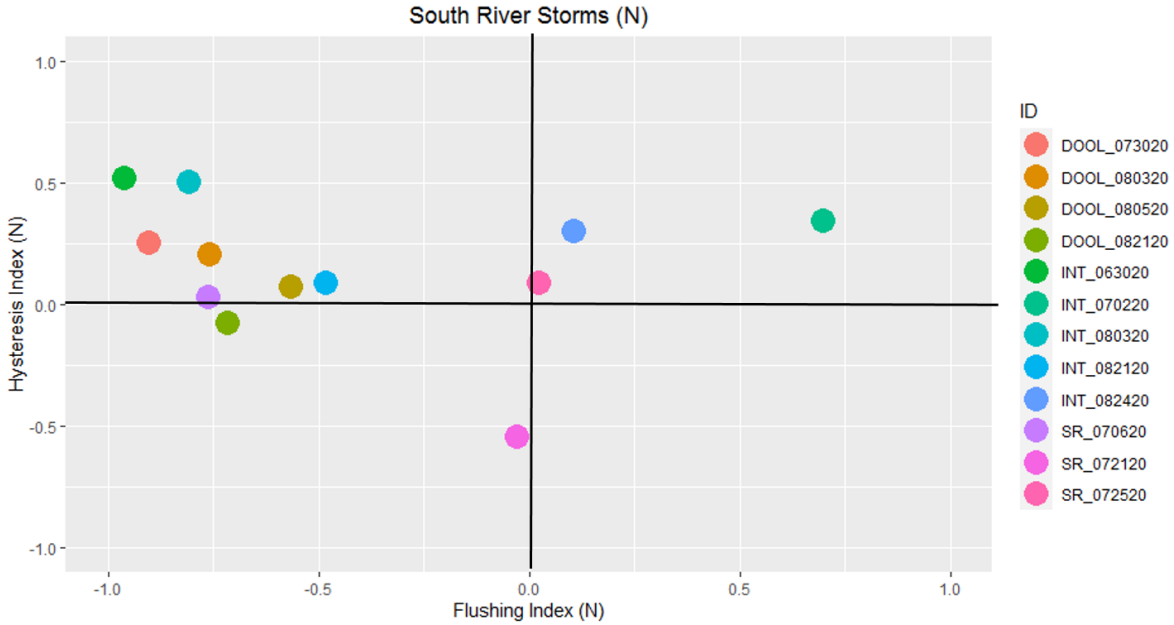

Figure 24: Storm events plotted with FI for NO_3^- on the x-axis and HI on the y-axis.

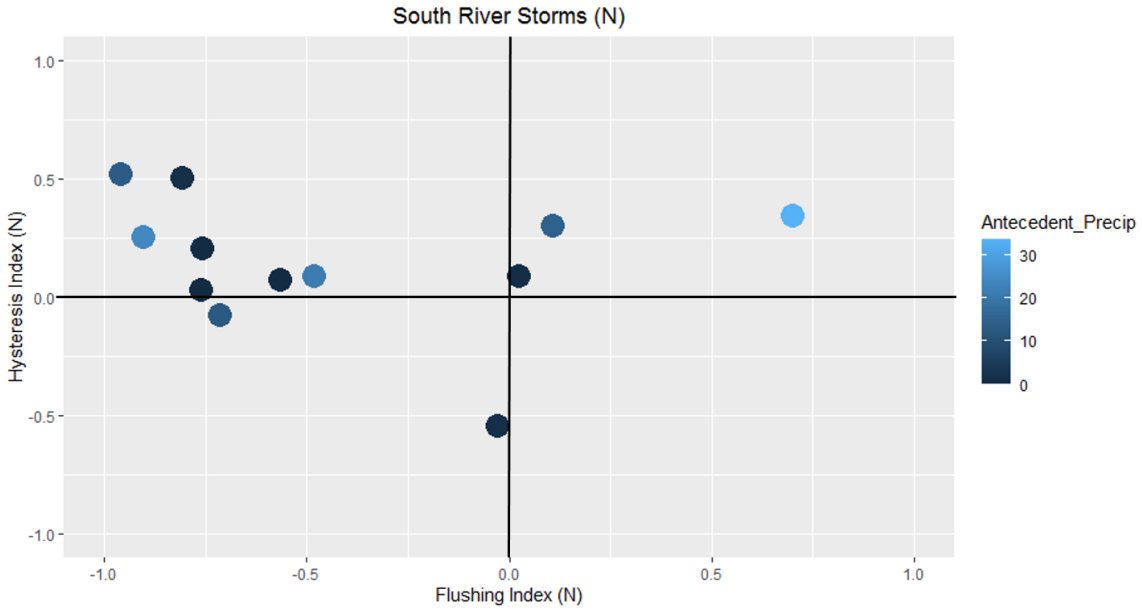

Figure 25: Storm events plotted with FI for NO_3^- on the x-axis and HI on the y-axis. Color gradient shows antecedent precipitation over 72 hours in mm.

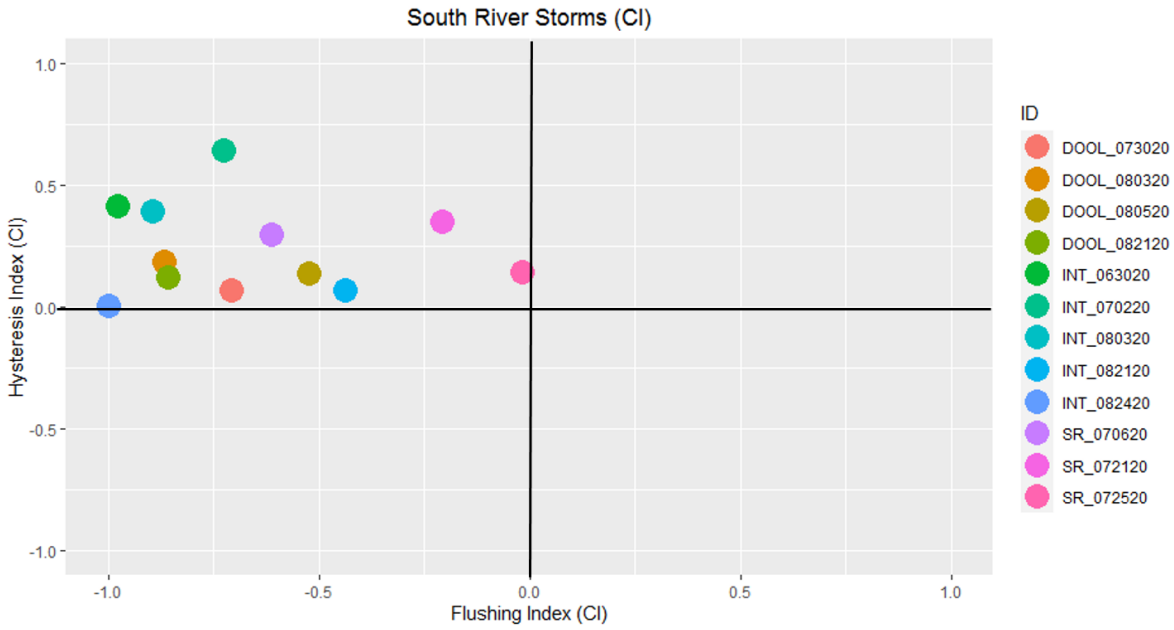

Figure 26: Storm events plotted with FI for Cl^- on the x-axis and HI on the y-axis.

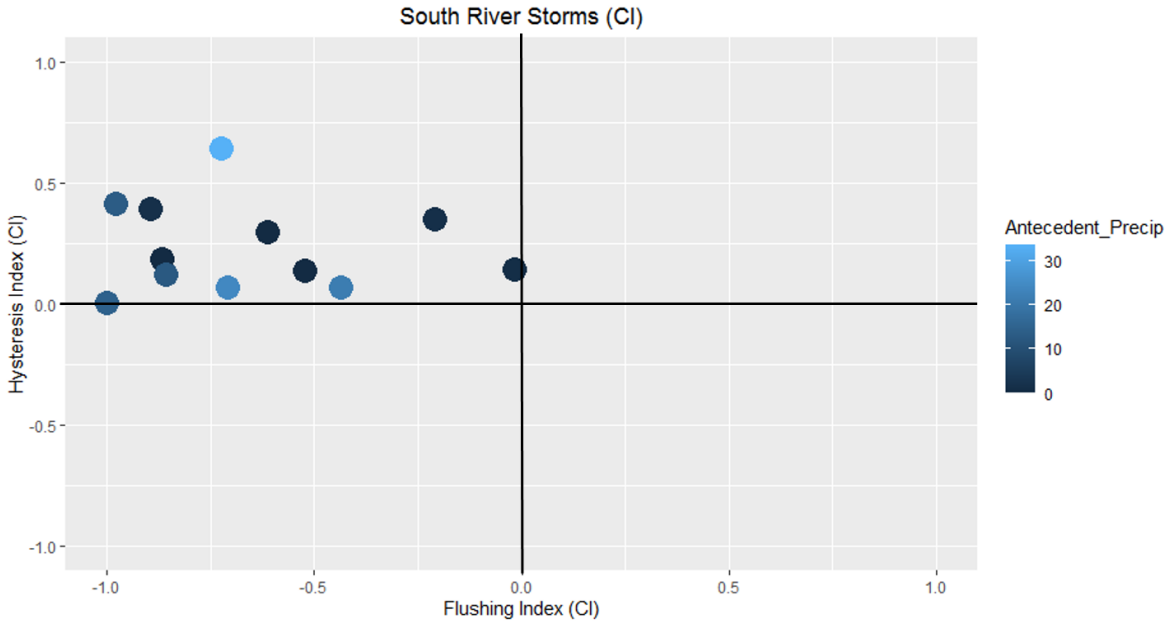

Figure 27:Storm events plotted with FI for Cl^- on the x-axis and HI on the y-axis. Color gradient shows antecedent precipitation over 72 hours in mm.

3.2.3 Long term C-Q relationships

Plots of discharge versus SPC at 15-minute temporal resolution for the entire sampling period (June 22, 2020 – September 30, 2020) for the 3 USGS gage sites (Fig. 28; Fig. 29; Fig. 30) showed a negative correlation. However, the plot for South River at Flakes Mill Road (Fig. 30) has much less spread/scatter than that of Intrenchment Creek at Constitution Road. Additionally, despite large differences in maximum discharge between the sites due to relative stream-order (South River at Flakes Mill Road exhibited the largest maximum discharge values, followed by Intrenchment Creek, then Doolittle Creek), all three sites exhibited similar log-transformed slopes (-0.23, -0.19, and -0.21 for South River, Intrenchment, and Doolittle, respectively).

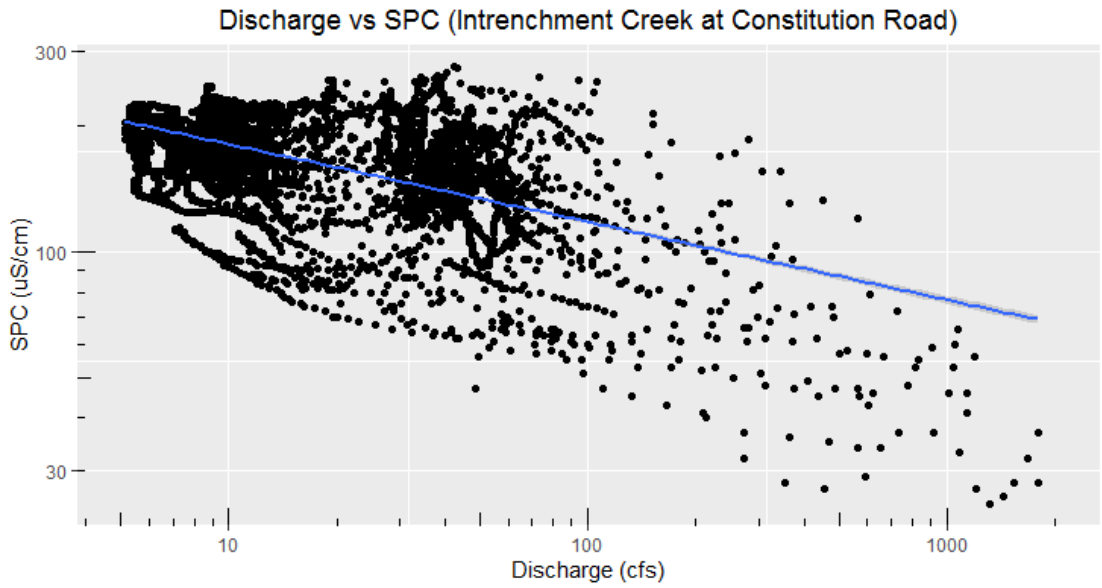

Figure 28:Scatterplot of discharge versus SPC at 15-minite intervals at Intrenchment Creek at Constitution Road (USGS 02203700) (June 22, 2020 – September 30, 2020). Both axes are log-scaled.

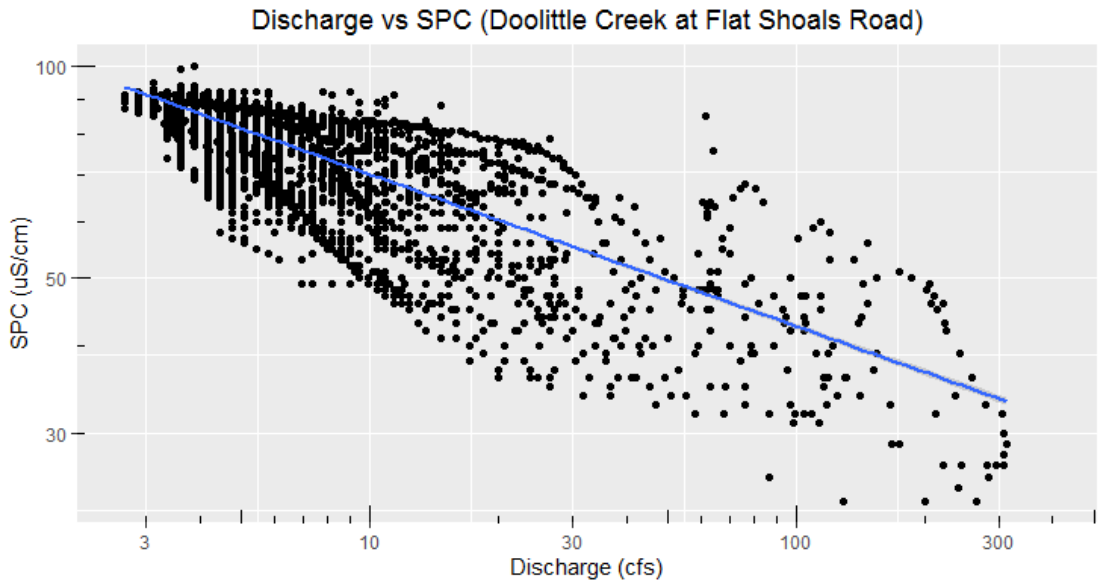

Figure 29:Scatterplot of Discharge versus SPC at 15-minute intervals at Doolittle Creek at Flat Shoals Road (USGS 02203831) (June 22, 2020 - September 30, 2020). Both axes are log-scaled.

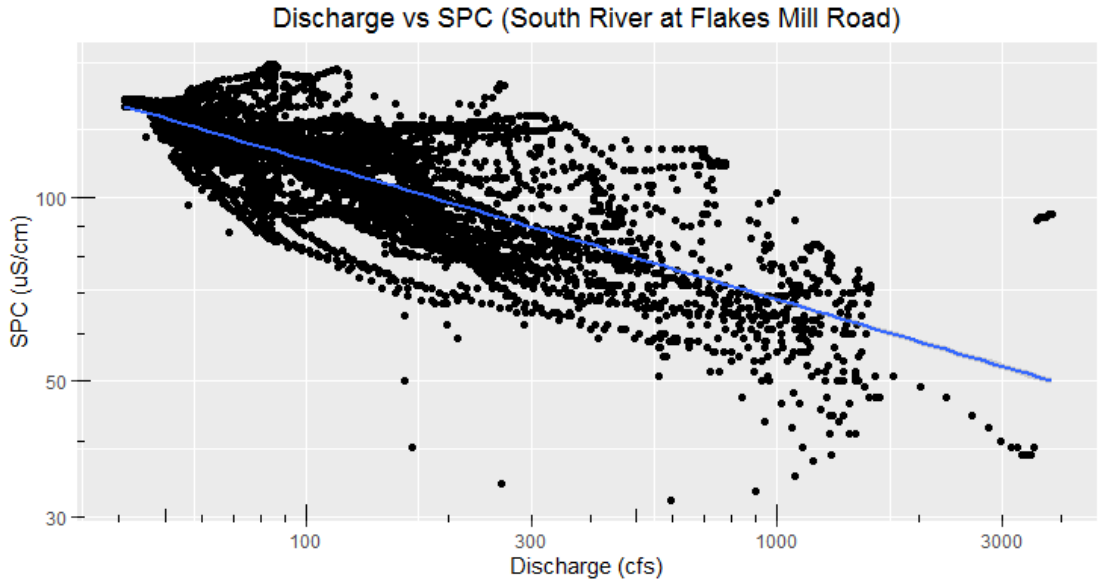

Figure 30: Scatterplot of discharge versus SPC at 15-minite intervals at South River at Flakes Mill Road (USGS 02203900) (June 22, 2020 – September 30, 2020). Both axes are log-scaled.

4 DISCUSSION

4.1 Baseflow

4.1.1 Baseflow characteristics and comparison with previous work

Studying the environment on the watershed scale has long been a crucial tool in ecosystem ecology because inputs and outputs of solutes, energy, and water can be more easily quantified and compared (Groffman et al., 2019). This spatial approach has been successfully employed in the relatively new fields of urban ecosystem ecology and hydrology, allowing researchers to more easily parse biogeochemical processes occurring in-stream that will ultimately affect downstream export (Koenig et al., 2017). Taken as a whole, the results of urban hydrologic and ecological studies to date have shown substantial site/reach scale heterogeneity within and among watersheds, both hydraulically and hydrochemically (Kaushal and Belt, 2012). Much of this heterogeneity has been attributed to spatially varying and temporally evolving levels of hydrologic connectivity at the site/reach scale, driven by engineered headwaters and other anthropogenic landscape alterations (Kaushal et al., 2008; Kaushal and Belt, 2012). Our objective for the baseflow component of this study was to characterize variation in baseflow hydrochemistry in headwater streams of the South River Watershed and relate it to differences in land use and other characteristics. Broadly, we found that headwaters in SRW exhibited a large degree of hydrochemical similarity relative to each other. However, a few sites (Such as BS-18) showed substantial temporal variability throughout the summer (Fig. 8; Fig. 9). Additionally, we found that at baseflow, NO_3^- and Cl^- concentrations were indeed significantly related to total percentages of urban and forested land (Fig. 13; Fig. 14; Fig. 15).

Furthermore, the results of this study appear largely similar to most other studies of urban baseflow and stormflow water quality at the watershed scale, particularly those performed within

similar physiographic settings to Atlanta (i.e., Piedmont settings). The differences in solute concentrations observed among sites can also likely be attributed to heterogenous hydrologic connectivity and spatially variable magnitudes of diffuse inputs. Baseflow hydrochemical results track relatively closely with prior studies of urban water quality. In multiple studies of low-order urban watersheds, baseflow NO_3^- values fell in a similar range to those observed in the SRW (Duncan et al., 2017; Tuttle et al., 2014; Mulholland et al., 2008). In particular, baseflow and stormflow values of most of the major ions measured proved highly similar to those previously measured at Peachtree Creek, a highly urbanized watershed in Atlanta located proximally northwest of SRW (Rose 2007; Rose, 2002). NO_3^- values were highly comparable between the sites and through time, with Rose (2002; 2007) reporting mean baseflow concentration of NO_3^- at Peachtree Creek of 0.62 mg/L, while mean stormflow concentration was 0.53 mg/L. In our study, mean baseflow NO_3^- concentration over all sites throughout the whole summer was approximately 0.64 mg/L (Fig. 8). Furthermore, Cl^- concentrations between the studies also tracked closely. At Peachtree Creek, Mean Cl^- concentrations were 7.8 mg/L at baseflow and 4.8 mg/L during stormflow in Peachtree Creek, while at SRW, the mean baseflow Cl^- concentration over all sites was approximately 6.3 mg/L (Fig. 9).

Other studies similar to ours have noted substantial variability in concentrations among superficially similar sites, even within the same catchment (Tuttle et al., 2014; Groffman et al., 2005). As such, the four sites with the lowest NO_3^- concentrations deserve individual consideration (see Fig. 8 and Fig. 9). BS-12 and BS-16 are the two sites associated with the small pond that exhibited substantially lower concentrations of both NO_3^- and Cl^- than other similar baseflow sites. These sites are unique in two ways: (1) they both have very low total drainage areas of less than 6 km^2, and (2) these catchments encompass two residential ponds, and the

percentage of open water in the drainage areas for these sites are 1.78% and 1.45%, respectively. Although both open water values are less than 2%, they are nonetheless substantially higher than all other sites in the study and will have direct impacts on downstream water chemistry. Given the presence of slow-moving, ponded water contributing to flow at both of these sites, one possible driver of the lower NO_3^- concentrations could be denitrification of inorganic N occurring in an anoxic hyporheic zone, which is a well-documented phenomenon in such conditions (Lautz and Fannelli, 2008; Mulholland et al., 2008; Kaushal et al., 2008). Average NO_3^- values decreased by more than 50% from BS-16 (0.23 mg N/L) to BS-12 (0.10 mg N/L), suggesting in-stream assimilation or removal of inorganic N along flow paths between the two sites (or another unknown input that is more dilute). Biological assimilation of inorganic N at this site may be driven by the pond receiving, especially if the two associated ponds receiving large amounts of sunlight during the summer months. Denitrification is not hypothesized as the driver for low nitrate at BS-16 (the inlet to the pond) because it did not have low DO concentrations (94-139% saturation). Low concentrations here could be driven by low nitrate in groundwater, a different source of water to the stream as shown by the low Cl^- concentrations, or limited upstream length over which biologic assimilation and decomposition can happen.

In addition to BS-12 and BS-16, two other baseflow sites (BS-2 and BS-7) showed abnormally low NO_3^- concentrations throughout the summer (Fig. 8). As with the pond-associated sites, BS-7 is associated with a very small drainage area (0.6 km^2, representing the smallest of all sites in the study). In contrast, BS-2 is associated with a moderate-sized drainage area (14.4 km^2). However, it is important to note that unlike the pond-associated sites, BS-2 and BS-7 did not exhibit abnormally low Cl^- concentrations, but rather just low NO_3^- values. As such, we can reasonably conclude that Cl^- is exhibiting a conservative behavior at these sites, while

NO_3^- concentrations are being influenced by in-stream processes. Counterintuitively, the drainage area associated with BS-7 is not only the smallest in the study, but it also consists of the highest total urban impervious land use (87.1%) of all sites studied, representing an outlier in terms of the general observed relationship between land use and water quality (Fig. 13). One plausible explanation for the discrepancy between solute concentrations and impervious land use is the tendency of low-order (and particularly first-order) streams to typically process over half of all N inputs into a watershed from the terrestrial environment, owing to their shallow depth profile and much higher surface area to volume ratio when compared to their larger order counterparts. These physical characteristics of headwater streams create an environment that is conducive for biogeochemical processing (Peterson et al., 2001).

BS-8 (Fig. 31) exhibited the second highest median NO_3^- concentration at baseflow (behind Intrenchment Creek). However, its median value for Cl^- fell in the moderate range between 4 and 8 mg/L This site is a first-order stream which was likely constructed and incorporated into a residential drainage system at the time of development. This is one common type of engineered headwater often present in urbanized systems (Kaushal and Belt, 2012). Although not channelized, BS-8 is located directly adjacent to a series of residential lawns. As such, one possible explanation for the high NO_3^- concentrations observed at this site is the prospect of localized fertilizer inputs. Multiple studies have shown that fertilizer can be a major source of N in surface water in both agricultural and urban watersheds (Huang et al., 2020). Furthermore, many studies of golf courses have shown that these highly fertilized and managed environments (which have similar characteristics to residential lawns) have the potential to export harmful amounts of N and P, although export can vary by multiple orders of magnitude (Bock et al., 2020).

Figure 31: Photograph of baseflow sampling site BS-8.

In addition to direct temporal and inter-site comparisons of baseflow concentration data, plots of the baseflow PCA results help to further parse potential factors driving the hydrochemistry of each site, as well as the system as a whole, by grouping the signal at each site on a given day into a broadly groundwater-driven (PC1-dominant) or metabolism-driven (PC2-dominant) category. Plotting PC1 versus PC2 for all baseflow observations, we see that BS-18, BS-17, BS-5 and BS-4 show substantial temporal variability in PC1 scores (Fig. 17). BS-5 and BS-17 are both sites located on the main stem South River itself, relatively close to the overall watershed outlet. As such, both have large drainage areas compared to the lower-order sites (approximately 156 km^2 and 108 km^2, respectively). A larger temporal variability in PC1 scores indicates that there may be a larger and/or longer surface water impact at these sites after storms.

This a plausible result, as prior studies have shown that higher-order streams tend to have a less flashy response than their headwater tributaries (Roodsari and Chandler, 2017). Additionally, BS-18 (Intrenchment Creek) also exhibited highly variable PC1 values (Fig. 17), as might be expected given the intermittent CSO inputs that are likely altering Cl^- concentrations and possibly other variables associated with PC1. As such, PC1 may not represent a true groundwater-driven signal here, as in other sites. In addition to the clear groundwater signal represented by PC1, PC2 is likely a metabolic signal, although this is a less clear designation. The associated variables for PC2 are NO_3^-, temperature, DO, and Mg^{2+}. Sites with relatively high variability in PC2 values over time include BS-8, BS-13, and BS-18 (Fig. 17; Fig. 18). Large PC2 values at BS-8 further support the idea that its high NO_3^- concentrations may be a result of fertilizer input, as anthropogenic external inputs have been shown to increase uptake and assimilation rates, thereby contributing to the stream metabolism (PC2) signal (Mulholland et al., 2009). However, one unclear result of the PCA is the presence of Mg^{2+} as a high-valued loading coefficient in PC2, as this ion is not usually associated with a metabolism-driven processes. We first believed that the abnormally high Mg^{2+} loading coefficient could be a result of the fact that that the two sites associated with the small residential pond (BS-12 and BS-16) exhibited abnormally high Mg^{2+} and Ca^+ concentrations throughout the summer compared with the other baseflow sites. However, many sites that did not have these elevated Mg^{2+} and Ca^+ concentrations also showed strong metabolism signals, such as BS-8, BS-17, and BS-18.

4.1.2 Land use controls on water quality in SRW

Significant relationships between mean NO_3^- and Cl^- concentrations and total urban/forested land use in the baseflow sites watersheds suggest that land use is indeed a control on solute concentrations. As such, our study is one of many that have shown the influence of ISC

on baseflow water quality (Arnold and Gibbons, 1996; Brabec et al., 2002). More specifically, our results are comparable with previous work in Atlanta in which solute concentrations increased with level of urban land use, and the urbanized sites exhibited significantly higher concentrations than the non-urbanized comparison sites (Rose, 2007). Despite the presence of these significant relationships, it is important to note that these simple models have relatively poor predictive power (all have R^2 values close to 0.3), indicating many things besides percent land use in the watershed are driving stream concentrations. Finally, the lack of significant relationships between 25m riparian land use and water quality also has interesting management implications. Prior work on the effectiveness of riparian buffers has shown that width is one of the most important factors controlling the level of N removal, with 50m buffers showing significantly more removal than 25m buffers (Mayer et al., 2007). As such, especially in urban headwaters, remediation and restoration projects must consider land use and development within the entire watershed, as opposed to exclusively in riparian buffers.

4.2 Stormflow

4.2.1 Controls on event-scale C-Q characteristics & context in urban C-Q framework

Evans and Davies (1998) related the form and rotational pattern of hysteresis loops to end-member component concentration rankings in 3-component and 2-component conservative mixing models of stormflow generation. They proposed that the determination of the relative concentrations of either “pre-event” and “event” water in the case of a 2-component model, or groundwater, “surface event water”, and soil water in the case of a 3-component model, could be determined through the classification of a given hysteresis loop into one of six categories based on its slope and rotational direction. As such, the relative importance of distinct hydrologic flow paths in the study catchment can also be inferred from this analysis.

Our broad objective for the stormflow component of this study was to examine relationships between stream discharge and concentrations of various solutes during storm events using a similar analytical framework as Evans and Davies (1998). We found that storm events captured in this study largely resemble the "C3" loop in the Evans and Davis typology (i.e., loops have a negative slope and clockwise rotational pattern) (Fig. 19; Fig. 20, Fig. 21, Fig. 22). This shape is associated with groundwater as the highest-concentration component of stormflow, followed by "surface event" water, with soil water as the lowest concentration (if using a 3-component model). Alternatively, if interpreting this as a 2-component system, this shape implies that "pre-event" water has a higher concentration than "event water." This tracks closely with one of the only previous urban C-Q studies performed in the Atlanta area (Rose, 2004), as well as other Piedmont settings, such as the eastern "upstate" regions of North and South Carolina and portions of Maryland (Tuttle, 2014; Duncan, 2017).

4.2.2 Context within existing long-term C-Q framework

Early C-Q studies in hydrology focused on the storm event scale (Johnson., 1982; Wailing, 1975; Glover et al., 1974). However, later studies have attempted to observe C-Q relationships beyond the storm event scale to seasonal, annual, or interannual scales (Koenig et al., 2017; Duncan et al., 2017). Godsey et al. (2009) found that despite well-defined C-Q responses observed on the shorter-term storm event-scale, analysis of long-term (i.e., annual and interannual) C-Q relationships showed that common geogenic solutes exhibited almost chemostatic (stationary) behavior in response to changing discharge. This is apparent when considering that in the data sets studied, discharge in a system varied by multiple orders or magnitude, while concentrations only varied by far less than one order of magnitude (Godsey et al., 2009). By plotting the long-term C-Q relationships at each of our gage sites using SPC data,

we saw a similar dynamic at play, despite the fact the SRW is a heavily urbanized catchment. Additionally, Godsey et al. (2019) showed that the slope of chemostatic C-Q relationship was more dilutive for tropical and subtropical climates. We see the same pattern in our subtropical climate, as seen in the high FI index values found in this study for storm events.

Additionally, the main possible explanation for the phenomenon of much higher scatter in our long-term C-Q diagram for Intrenchment Creek at Constitution Road (USGS 02203700) is that this site experiences periodic inputs due to periodic use of the upstream treatment plant, unlike sites that receive constant WWTP effluent (Ledford and Toran 2020). Additionally, our sampling of one of these events showed that Cl^- levels rose during the outfall event, suggesting that effluent from the CSO facility may elevate the normal conductivity signal. This is a hot spot of heterogeneity in baseflow in this system that is assimilated with distance, as no other sites show the same variability.

4.3 Context within urban watershed continuum

The urban watershed continuum framework expands on the urban stream syndrome concept of systematic ecological and hydrologic degradation in urban settings (Walsh et al., 2005; Kaushal and Belt, 2012). It does so by integrating observations of four spatiotemporal dimensions (lateral, longitudinal, vertical, and temporal), as well as emphasizing the importance of evolving hydrologic connectivity of flow paths in urban systems through time. Our baseflow study contributes to this framework by showing key interactions in urban headwater streams between surrounding land use (Fig. 13; Fig. 14; Fig. 15) and evolving hydrologic connectivity in anthropogenically altered or engineered headwaters. Despite outlier sites associated with point-sources such as BS-18, as well as some spatial variability in solute concentrations among the first-order sites, we see an integrated baseflow signal observed at the watershed outlet (BS-1,

South River at Flakes Mill Road) as well as sites on the main stem of the South River close to the outlet (i.e., BS-04, BS-05 BS-17). With the knowledge that these integrated signals are less variable and encompass the heterogeneity of the upstream sites, monitoring efforts to understand major anion and cation chemistry can be focused on such outlets in urban settings where monitoring resources are scarce without loss of information. Regarding our second objective, storm events observed in this study generally have a relatively homogenous response (i.e. the majority of events exhibited dilution and clockwise rotation) despite the heterogeneity that would be expected in a highly urbanized watershed (Table 8).

5 CONCLUSION

Overall a few general insights can be gleaned from this study. First, in our study watershed, urban land use and ISC are related to mean NO_3^- and Cl^- concentrations at baseflow. We find that the main drivers of spatial and temporal variability in baseflow concentrations are related to differences in groundwater contribution or concentration at each site and the metabolic activity of the stream. But, overall, there is minimal variability in baseflow chemistry across the headwaters, indicating a homogeneity in a system that is often assumed to be highly heterogeneous. This is supported by the storm event study as well, with our sampled storms showed largely dilutive behavior and clockwise rotation and similar C-Q slopes for nested watersheds. Anomalous N flushing in 3 storms may be driven by antecedent precipitation. Taking our baseflow and stormflow data together, we can conclude that SRW is a source-limited system where groundwater represents the highest-concentration component of stormflow and drives baseflow concentrations with surprising homogeneity across the system. Such localized information could potentially play a significant role in future stream mitigation efforts in the urban landscapes.

REFERENCES

Aguilera, R., & Melack, J. M. (2018). Concentration-discharge responses to storm events in coastal California watersheds. *Water Resources Research*, *54*(1), 407-424.

Arnold Jr, C. L., & Gibbons, C. J. (1996). Impervious surface coverage: the emergence of a key environmental indicator. *Journal of the American planning Association*, *62*(2), 243-258.

Baker, E. B., & Showers, W. J. (2019). Hysteresis analysis of nitrate dynamics in the Neuse River, NC. *Science of the Total Environment*, *652*, 889-899.

Baker, L. A., Hope, D., Xu, Y., Edmonds, J., & Lauver, L. (2001). Nitrogen balance for the Central Arizona–Phoenix (CAP) ecosystem. *Ecosystems*, *4*(6), 582-602.

Basu, N. B., Destouni, G., Jawitz, J. W., Thompson, S. E., Loukinova, N. V., Darracq, A., ... & Rao, P. S. C. (2010). Nutrient loads exported from managed catchments reveal emergent biogeochemical stationarity. *Geophysical Research Letters*, *37*(23).

Basu, N. B., Rao, P. S. C., Winzeler, H. E., Kumar, S., Owens, P., & Merwade, V. (2010). Parsimonious modeling of hydrologic responses in engineered watersheds: Structural heterogeneity versus functional homogeneity. *Water resources research*, *46*(4).

Bell, C. D., McMillan, S. K., Clinton, S. M., & Jefferson, A. J. (2017). Characterizing the effects of stormwater mitigation on nutrient export and stream concentrations. *Environmental management*, *59*(4), 604-618.

Bhaskar, A. S., Hopkins, K. G., Smith, B. K., Stephens, T. A., & Miller, A. J. (2020). Hydrologic signals and surprises in US streamflow records during urbanization. *Water Resources Research*, *56*(9), e2019WR027039.

Bieroza, M. Z., & Heathwaite, A. L. (2015). Seasonal variation in phosphorus concentration–discharge hysteresis inferred from high-frequency in situ monitoring. *Journal of Hydrology*, *524*, 333-347.

Bloom, D. E., Canning, D., & Fink, G. (2008). Urbanization and the wealth of nations. *Science*, *319*(5864), 772-775.

Bock, E. M., & Easton, Z. M. (2020). Export of nitrogen and phosphorus from golf courses: A review. *Journal of environmental management*, *255*, 109817.

Bowes, M. J., House, W. A., & Hodgkinson, R. A. (2003). Phosphorus dynamics along a river continuum. *Science of the total environment*, *313*(1-3), 199-212.

Bowes, M. J., House, W. A., Hodgkinson, R. A., & Leach, D. V. (2005). Phosphorus–discharge hysteresis during storm events along a river catchment: the River Swale, UK. *Water research*, *39*(5), 751-762.

Brabec, E., Schulte, S., & Richards, P. L. (2002). Impervious surfaces and water quality: a review of current literature and its implications for watershed planning. *Journal of planning literature*, *16*(4), 499-514.

Carey, R. O., Wollheim, W. M., Mulukutla, G. K., & Mineau, M. M. (2014). Characterizing storm-event nitrate fluxes in a fifth order suburbanizing watershed using in situ sensors. *Environmental science & technology*, *48*(14), 7756-7765.

Carroll, K. P., Rose, S., & Peters, N. E. (2007). Concentration/discharge hysteresis analysis of storm events at the Panola mountain research watershed, Georgia, USA. Georgia Institute of Technology.

Chanat, J. G., Rice, K. C., & Hornberger, G. M. (2002). Consistency of patterns in concentration-discharge plots. *Water Resources Research*, *38*(8), 22-1.

City of Atlanta (2005). Custer Avenue Combined Sewer Overflow (CSO) Storage & Dechlorination Facility. Accessed March 2020.

City of Atlanta (2019). East Area Facilities Summary of CSS Discharge Events January – December 2019. Accessed March 2020.

Diem, J. E., Hill, T. C., & Milligan, R. A. (2018). Diverse multi-decadal changes in streamflow within a rapidly urbanizing region. Journal of Hydrology, 556, 61-71.

Duncan, J. M., Welty, C., Kemper, J. T., Groffman, P. M., & Band, L. E. (2017). Dynamics of nitrate concentration-discharge patterns in an urban watershed. *Water Resources Research*, *53*(8), 7349-7365.

Evans, C., & Davies, T. D. (1998). Causes of concentration/discharge hysteresis and its potential as a tool for analysis of episode hydrochemistry. *Water Resources Research*, *34*(1), 129-137.

Frick, E. A. (1998). *Water quality in the Apalachicola-Chattahoochee-Flint River basin, Georgia, Alabama, and Florida, 1992-95* (No. 1164-1170). US Geological Survey.

Georgia EPD (2020). Summary Page: City of Atlanta – East Area Combined Sewer Overflow Facility NPDES Permit. Accessed March 2020.

Godsey, S. E., Hartmann, J., & Kirchner, J. W. (2019). Catchment chemostasis revisited: Water quality responds differently to variations in weather and climate. *Hydrological Processes*, *33*(24), 3056-3069.

Godsey, S. E., Kirchner, J. W., & Clow, D. W. (2009). Concentration–discharge relationships reflect chemostatic characteristics of US catchments. *Hydrological Processes: An International Journal*, *23*(13), 1844-1864.

Gregory, M. B., & Frick, E. A. (2000). *Fecal-coliform bacteria concentrations in streams of the Chattahoochee River National Recreation Area, Metropolitan Atlanta, Georgia, May-October 1994 and 1995* (No. 4139). US Geological Survey.

Groffman, P. M., Band, L. E., Belt, K. T., Bettez, N. D., Bhaskar, A., Doheny, E., ... & Welty, C. (2019). Applying the Watershed Approach to Urban Ecosystems. *Science for the Sustainable City: Empirical Insights from the Baltimore School of Urban Ecology*, 155.

Groffman, P. M., Dorsey, A. M., & Mayer, P. M. (2005). N processing within geomorphic structures in urban streams. *Journal of the North American Benthological Society*, *24*(3), 613-

625.

Gwenzi, W., Chinyama, S. R., & Togarepi, S. (2017). Concentration-discharge patterns in a small urban headwater stream in a seasonally dry water-limited tropical environment. *Journal of Hydrology*, *550*, 12-25.

Hornberger, G. M., Scanlon, T. M., & Raffensperger, J. P. (2001). Modelling transport of dissolved silica in a forested headwater catchment: the effect of hydrological and chemical time scales on hysteresis in the concentration–discharge relationship. *Hydrological processes*, *15*(10), 2029-2038.

Huang, Y., Huang, J., Ervinia, A., & Duan, S. (2020). Tracking riverine nitrate sources under changing land use pattern and hydrologic regime. *Marine Pollution Bulletin*, *152*, 110884.

Johnson, F. A., & East, J. W. (1982). Cyclical relationships between river discharge and chemical concentration during flood events. *Journal of Hydrology*, *57*(1), 93-106.

Kaushal, S. S., & Belt, K. T. (2012). The urban watershed continuum: evolving spatial and temporal dimensions. *Urban Ecosystems*, *15*(2), 409-435.

Kaushal, S. S., Groffman, P. M., Mayer, P. M., Striz, E., & Gold, A. J. (2008). Effects of stream restoration on denitrification in an urbanizing watershed. *Ecological Applications*, *18*(3), 789-804.

Koenig, L. E., Shattuck, M. D., Snyder, L. E., Potter, J. D., & McDowell, W. H. (2017). Deconstructing the effects of flow on DOC, nitrate, and major ion interactions using a high-frequency aquatic sensor network. *Water Resources Research*, *53*(12), 10655-10673.

Lautz, L. K., & Fanelli, R. M. (2008). Seasonal biogeochemical hotspots in the streambed around restoration structures. *Biogeochemistry*, *91*(1), 85-104.

Law, N., Band, L., & Grove, M. (2004). Nitrogen input from residential lawn care practices in suburban watersheds in Baltimore County, MD. *Journal of Environmental Planning and Management*, *47*(5), 737-755.

Ledford, S. H., Lautz, L. K., Vidon, P. G., & Stella, J. C. (2017). Impact of seasonal changes in stream metabolism on nitrate concentrations in an urban stream. *Biogeochemistry*, *133*(3), 317-3

Ledford, S. H., Zimmer, M., & Payan, D. (2020). Anthropogenic and Biophysical Controls on Low Flow Hydrology in the Southeastern United States. *Water Resources Research*, *56*(9), e2020WR027098.

Mayer, P. M., Reynolds Jr, S. K., McCutchen, M. D., & Canfield, T. J. (2007). Meta-analysis of nitrogen removal in riparian buffers. *Journal of environmental quality*, *36*(4), 1172-1180.

Meyer, J. L., Paul, M. J., & Taulbee, W. K. (2005). Stream ecosystem function in urbanizing landscapes. *Journal of the North American Benthological Society*, *24*(3), 602-612.

Mulholland, P. J., Helton, A. M., Poole, G. C., Hall, R. O., Hamilton, S. K., Peterson, B. J., ... & Thomas, S. M. (2008). Stream denitrification across biomes and its response to anthropogenic nitrate loading. *Nature*, *452*(7184), 202-205.

O'Driscoll, M., Clinton, S., Jefferson, A., Manda, A., & McMillan, S. (2010). Urbanization effects on watershed hydrology and in-stream processes in the southern United States. *Water*, *2*(3), 605-648.

Paul, M. J., & Meyer, J. L. (2001). Streams in the urban landscape. *Annual review of Ecology and Systematics*, *32*(1), 333-365.

Peterson, B. J., Wollheim, W. M., Mulholland, P. J., Webster, J. R., Meyer, J. L., Tank, J. L., ... & Morrall, D. D. (2001). Control of nitrogen export from watersheds by headwater streams. *Science*, *292*(5514), 86-90.

R Core Team (2020). R: A language and environment for statistical computing. R Foundation for Statistical Computing, Vienna, Austria. URL https://www.R-project.org/.

Roodsari, B. K., & Chandler, D. G. (2017). Distribution of surface imperviousness in small urban catchments predicts runoff peak flows and stream flashiness. *Hydrological Processes*, *31*(17), 2990-3002.

Rose, L. A., Karwan, D. L., & Godsey, S. E. (2018). Concentration–discharge relationships describe solute and sediment mobilization, reaction, and transport at event and longer timescales. *Hydrological Processes*, *32*(18), 2829-2844.

Rose, S. (2002). Comparative major ion geochemistry of Piedmont streams in the Atlanta, Georgia region: possible effects of urbanization. *Environmental Geology*, *42*(1), 102-113.

Rose, S. (2003). Comparative solute–discharge hysteresis analysis for an urbanized and a 'control basin' in the Georgia (USA) Piedmont. *Journal of Hydrology*, *284*(1-4), 45-56.

Rose, S. (2007). The effects of urbanization on the hydrochemistry of base flow within the Chattahoochee River Basin (Georgia, USA). *Journal of Hydrology*, *341*(1-2), 42-54.

Rose, S., & Peters, N. E. (2001). Effects of urbanization on streamflow in the Atlanta area (Georgia, USA): a comparative hydrological approach. Hydrological Processes, 15(8), 1441-1457.

Scanlon, T. M., Raffensperger, J. P., & Hornberger, G. M. (2001). Modeling transport of dissolved silica in a forested headwater catchment: Implications for defining the hydrochemical response of observed flow pathways. *Water Resources Research*, *37*(4), 1071-1082.

Shaharudin, S. M., Ahmad, N., Zainuddin, N. H., & Mohamed, N. S. (2018). Identification of rainfall patterns on hydrological simulation using robust principal component analysis. *Indonesian Journal of Electrical Engineering and Computer Science (IJEECS)*, *11*(3), 1162-1167.

Shields, C. A., Band, L. E., Law, N., Groffman, P. M., Kaushal, S. S., Savvas, K., ... & Belt, K. T. (2008). Streamflow distribution of non–point source nitrogen export from urban-rural catchments in the Chesapeake Bay watershed. *Water Resources Research*, *44*(9).

Singh, P. K., Kumar, V., Purohit, R. C., Kothari, M., & Dashora, P. K. (2009). Application of principal component analysis in grouping geomorphic parameters for hydrologic modeling. *Water resources management*, *23*(2), 325-339.

Smith, S. V., Swaney, D. P., Talaue-Mcmanus, L., Bartley, J. D., Sandhei, P. T., McLAUGHLIN, C. J., ... & Wulff, F. (2003). Humans, hydrology, and the distribution of inorganic nutrient loading to the ocean. *BioScience*, *53*(3), 235-245.

Thompson, S. E., Basu, N. B., Lascurain, J., Aubeneau, A., & Rao, P. S. C. (2011). Relative dominance of hydrologic versus biogeochemical factors on solute export across impact gradients. *Water Resources Research*, *47*(10).

Tuttle, A. K., McMillan, S. K., Gardner, A., & Jennings, G. D. (2014). Channel complexity and nitrate concentrations drive denitrification rates in urban restored and unrestored streams. *Ecological engineering*, *73*, 770-777.

USGS (2019). National Hydrography Dataset (ver. USGS National Hydrography Dataset Best Resolution (NHD) for Hydrologic Unit (HU) 4 - 2001 (accessed April, 2020)

USGS Site Data: Stream Gage 02203700. https://www.waterqualitydata.us/provider/NWIS/USGS-GA/USGS-02203700/ (accessed April 10, 2020).

USGS Site Data: Stream Gage 02203831. https://www.waterqualitydata.us/provider/NWIS/USGS-GA/USGS-02203831/ (accessed April 10, 2020).

USGS Site Data: Stream Gage 02203900. https://www.waterqualitydata.us/provider/NWIS/USGS-GA/USGS-02203900/ (accessed April 10, 2020).

Vitousek, P. M., Aber, J. D., Howarth, R. W., Likens, G. E., Matson, P. A., Schindler, D. W., ... & Tilman, D. G. (1997). Human alteration of the global nitrogen cycle: sources and consequences. *Ecological applications*, *7*(3), 737-750.

Walling, D. E., & Foster, I. D. L. (1975). Variations in the natural chemical concentration of river water during flood flows, and the lag effect: some further comments. *Journal of Hydrology*, *26*(3-4), 237-244.

Walsh, C. J., Roy, A. H., Feminella, J. W., Cottingham, P. D., Groffman, P. M., & Morgan, R. P. (2005). The urban stream syndrome: current knowledge and the search for a cure. *Journal of the North American Benthological Society*, *24*(3), 706-723.

Wickham H (2016). *ggplot2: Elegant Graphics for Data Analysis*. Springer-Verlag New York. ISBN 978-3-319-24277-4, https://ggplot2.tidyverse.org.

Wollheim, W. M., Pellerin, B. A., Vörösmarty, C. J., & Hopkinson, C. S. (2005). N retention in urbanizing headwater catchments. *Ecosystems*, *8*(8), 871-884.

Zuecco, G., Penna, D., Borga, M., & van Meerveld, H. J. (2016). A versatile index to characterize hysteresis between hydrological variables at the runoff event timescale. *Hydrological Processes*, *30*(9), 1449-1466.

APPENDICES

Appendix A: Land use data

NLCD 2016 Land Use Classes as percentage of total drainage area for each baseflow sampling site. Additionally, ISC is categorized into different types and also presented as percentage of total drainage area.

Land Use (NLCD 2016)	BS-1	BS-2	BS-3	BS-4	BS-5	BS-6	BS-7	BS-8	BS-9	BS-10	BS-11	BS-12	BS-13	BS-14	BS-15	BS-16	BS-17	BS-18
Open Water	0.31	0.73	0.31	0.33	0.25	0.22	0.00	0.00	0.02	0.02	0.09	1.78	0.30	0.08	0.60	1.45	0.18	0.30
Dev, Open	26.93	17.5	26.42	24.31	35.55	36.14	41.73	30.73	41.21	41.21	31.68	26.23	21.25	22.18	38.32	26.32	20.50	21.25
Dev, Low	27.02	21.2	27.32	26.58	30.65	29.38	41.12	26.65	30.51	30.51	29.42	28.08	29.73	24.55	26.53	27.48	26.88	29.73
Dev, Med	11.41	4.45	12.87	14.03	7.91	9.31	1.67	5.66	6.04	6.04	9.34	4.80	17.60	11.96	7.64	4.58	16.73	17.60
Dev, High	8.33	0.49	9.90	11.47	3.16	4.09	2.58	2.23	2.18	2.18	3.99	0.88	12.83	18.61	5.25	0.92	14.75	12.83
Barren Land	0.25	1.62	0.19	0.23	0.02	0.04	9.41	0.00	0.00	0.00	0.10	0.11	0.85	0.16	0.03	0.11	0.30	0.85
Deciduous Forest	9.75	22.1	8.64	9.12	6.52	4.11	3.49	12.07	1.37	1.37	6.24	20.24	6.95	5.70	6.12	21.07	9.25	6.95
Evergreen Forest	8.35	9.53	7.76	7.23	10.00	9.68	0.00	16.81	13.03	13.03	10.22	10.34	3.44	13.66	10.57	10.49	5.58	3.44
Mixed Forest	3.82	2.37	3.87	3.65	4.61	5.22	0.00	0.00	5.23	5.23	6.03	3.23	4.01	3.01	3.88	3.29	3.26	4.01
Shrub/Scrub	0.22	0.53	0.15	0.18	0.06	0.08	0.00	0.00	0.05	0.05	0.11	0.72	0.33	0.04	0.02	0.75	0.17	0.33
Grassland/Herb	0.75	6.61	0.29	0.34	0.11	0.05	0.00	0.00	0.00	0.00	0.35	0.67	0.08	0.00	0.16	0.65	0.31	0.08
Pasture/Hay	1.41	6.65	1.00	1.11	0.53	0.68	0.00	3.99	0.37	0.37	1.21	2.32	2.59	0.04	0.82	2.27	1.02	2.59
Woody Wetlands	1.41	6.16	1.24	1.38	0.63	1.00	0.00	1.86	0.00	0.00	1.09	0.59	0.03	0.00	0.06	0.62	1.02	0.03
Emergent Herbaceous Wetland	0.04	0.03	0.04	0.05	0.00	0.00	0.00	0.00	0.00	0.00	0.13	0.00	0.00	0.00	0.00	0.00	0.03	0.00
Total Forested	21.93	34.0	20.26	19.99	21.13	19.01	3.49	28.88	19.63	19.63	22.50	33.81	14.40	22.38	20.57	34.85	18.09	14.40
Total Urban	73.68	43.6	76.51	76.39	77.26	78.92	87.10	65.27	79.93	79.93	74.43	60.00	81.42	77.31	77.73	59.30	78.86	81.42
Not Impervious	26.32	54.9	23.44	23.66	21.57	21.17	27.05	37.99	17.78	16.69	26.36	41.22	20.80	22.42	22.64	41.54	21.13	18.58
Primary road	1.83	0.00	2.33	2.31	2.62	1.49	0.00	0.00	0.00	0.00	2.42	0.00	1.36	4.31	2.24	0.00	2.56	2.35
Secondary road	5.36	2.95	5.76	6.08	4.25	4.15	4.63	1.95	4.38	2.65	5.01	3.63	6.16	5.33	5.91	3.59	6.58	8.34
Tertiary road	20.03	13.8	20.10	19.25	23.95	24.01	18.15	21.17	27.90	28.80	22.85	18.59	22.55	24.08	21.50	18.27	19.03	21.99
Non-road impervious	46.46	28.4	48.37	48.71	47.61	49.17	50.18	38.90	49.93	51.86	43.36	36.56	49.13	43.86	47.71	36.59	50.69	48.74
Total Impervious	73.68	45.1	76.56	76.34	78.43	78.83	72.95	62.01	82.22	83.31	73.64	58.78	79.20	77.58	77.36	58.46	78.87	81.42

Areal land use percentages (NLCD) calculated using a 25m buffer around the stream in each watershed.

Land Use (25m Buffer)	BS-1	BS-2	BS-3	BS-4	BS-5	BS-6	BS-7	BS-8	BS-9	BS-10	BS-11	BS-12	BS-13	BS-14	BS-15	BS-16	BS-17	BS-18
Open Water	1.0	0.2	1.1	1.1	0.4	0.0	0.0	0.0	0.0	0.0	0.4	4.8	4.8	0.6	1.5	0.0	0.1	0.0
Developed, Open	24.4	10.3	27.4	24.2	34.8	27.6	39.1	78.8	31.6	44.1	22.2	35.4	35.4	25.9	33.6	8.5	20.4	31.3
Developed, Low	13.9	5.5	14.6	13.1	19.9	10.4	4.3	7.7	8.6	15.0	16.1	17.5	17.5	12.1	12.4	0.0	15.8	23.5
Developed, Med	4.5	0.9	4.7	4.8	2.7	0.9	4.3	1.9	0.4	2.4	5.7	2.7	2.7	5.2	2.8	0.0	7.4	4.5
Developed, High	1.7	0.0	2.7	2.2	0.1	0.4	0.0	0.0	0.0	0.0	3.0	0.6	0.6	2.3	1.7	0.0	4.2	0.9
Barren Land	0.1	1.2	0.1	0.0	0.0	0.0	0.0	0.0	0.0	0.0	0.0	0.0	0.0	0.0	0.0	0.0	0.2	0.1
Deciduous Forest	18.8	36.4	13.3	17.0	14.0	6.7	13.0	3.8	5.7	5.7	7.0	6.3	6.3	14.9	14.7	35.2	18.5	14.7
Evergreen Forest	12.6	5.0	13.7	12.9	10.6	23.3	21.7	3.8	28.3	17.0	20.9	21.5	21.5	20.1	19.4	12.7	11.4	4.6
Mixed Forest	12.9	2.6	12.9	14.6	14.2	20.4	17.4	3.8	25.4	15.4	18.6	10.8	10.8	19.0	11.3	18.3	12.0	17.7
Shrub/Scrub	0.2	1.0	0.3	0.2	0.1	0.0	0.0	0.0	0.0	0.4	0.1	0.0	0.0	0.0	0.0	8.5	0.2	0.1
Grassland/Herb	1.0	7.0	0.1	0.3	0.0	0.0	0.0	0.0	0.0	0.0	0.0	0.0	0.0	0.0	0.0	0.0	0.3	0.0
Pasture/Hay	1.6	6.0	1.9	1.6	0.3	0.0	0.0	0.0	0.0	0.0	3.8	0.4	0.4	0.0	2.1	0.0	2.2	2.6
Woody Wetlands	7.2	23.7	7.1	7.8	2.8	10.2	0.0	0.0	0.0	0.0	2.2	0.0	0.0	0.0	0.4	16.9	7.2	0.0
Emergent Herb Wetland	0.1	0.2	0.2	0.3	0.0	0.0	0.0	0.0	0.0	0.0	0.0	0.0	0.0	0.0	0.0	0.0	0.2	0.0
Total Urban	44.4	16.7	49.3	44.2	57.5	39.3	47.8	88.5	40.6	61.5	46.9	56.3	56.3	45.4	50.6	8.5	47.8	60.1
Total Forest	44.4	44.0	39.9	44.5	38.8	50.4	52.2	11.5	59.4	38.1	46.6	38.5	38.5	54.0	45.4	66.2	41.9	37.0